Doctoral Thesis

Charge Disproportionation State in Organic Conductors

Kazuhiro Katono

Department of Applied Physics

Hokkaido University

2015

Contents

Chapter 1

Introduction

1.1 Wigner Crystal

Wigner crystal is an electron localized state due to the long range Coulomb interaction between electrons, which has been predicted theoretically by E. Wigner [1]. He suggested that electrons are localized whenever the electron density is lower than a critical value. First, let us consider the electron system with low electron density in the space without periodic potential. The energy of i-th electron, E_i, is given by a sum of the kinetic energy and Coulomb potential between electrons as below,

$$E_i = \frac{\hbar^2 k_i^2}{2m} + \sum_{j,j\neq i} \frac{e^2}{|\boldsymbol{r}_i - \boldsymbol{r}_j|}, \tag{1.1}$$

where m and e are the mass and the charge of an electron, k_i is the wavenumber of the i-th electron, $\boldsymbol{r}_i$ and $\boldsymbol{r}_j$ are the position of the i-th and j-th electron, respectively.

Electrons are expected to be localized by the Coulomb interaction between themselves when the lowest Coulomb energy is larger than the highest kinetic energy *i.e.* the Fermi energy, regardless of the dimension of an electron system. The electron localization is specified by the average distance between electrons. The Fermi energy is given by $\frac{\hbar^2 k_{\rm F}^2}{2m}$ as a function of Fermi wavenumber $k_{\rm F}$. Taking into account the relation of electron density and the average distance between electrons in the D dimensional electron system $n = \frac{1}{r_{\rm av}^D}$, the Fermi wavenumber of the D dimensional electron system is

$$k_{\rm F} = \frac{2\pi}{(C_D)^{\frac{1}{D}}} n_D^{\frac{1}{D}} = \frac{2\pi}{(C_D)^{\frac{1}{D}}} \frac{1}{r_{\rm av}}, \tag{1.2}$$

where C_D is the coefficient of the volume of the D dimensional sphere when the volume V_D is written as $C_D r_{\rm av}^D$, n_D is the electron density in D dimensional system and we used the relation between n_D and the averaged distance between electrons $r_{\rm av}$ as $n_D = \frac{1}{(r_{\rm av})^D}$. The kinetic energy of the electron with $k_{\rm F}$ is

$$E_{\rm F} = \frac{\hbar^2 k_{\rm F}^2}{2m} = \frac{2\pi^2\hbar^2}{(C_D)^{\frac{2}{D}}} \frac{1}{r_{\rm av}^2}. \tag{1.3}$$

On the other hand, the lowest Coulomb energy is proportional to $\frac{e^2}{r_{\rm av}}$ since it takes the lowest energy when all distances between neighboring electrons are the same. Focusing on the average distance dependence of the kinetic and Coulomb energy, the kinetic energy is proportional to $\frac{1}{r_{\rm av}^2}$ whereas the Coulomb energy is proportional to $\frac{1}{r_{\rm av}}$. Therefore, the lowest Coulomb energy definitely exceeds the Fermi energy for larger $r_{\rm av}$. Then electrons are crystallized to reduce the Coulomb interaction.

Wigner crystal has been observed experimentally in homogeneous 2D electron systems e.g. electron systems on surface of liquid helium with 2×10^9 cm^{-2} of electron density [2, 3]. In the electron system on the surface, two dimensional electron system without periodic potential is realized since electrons lie on the surface at distances much larger than $\Delta r_{\rm avg}$.

Even in electron system with crystal lattice, electron localized states due to the strong electron-electron interaction have been found such as Mott insulator [4] and charge order [5]. Especially, organic conductors have been well-known as the electron systems with the strong long-rage Coulomb interaction [6]. In organic conductor, the localized state of electrons due to the long range Coulomb interaction (charge order) was also found. It has been suggested that charge order in quasi 1D system is a "Wigner crystal on lattice". Charge order in quasi 2D system was also found, it provides new stage for study of Wigner crystal.

1.2 Organic conductors

Organic conductors [6] are expected to be a system which provides the stages to study the electron localized state due to the strong electron-electron interaction [6]. Organic conductor is a sort of change transfer salts. Most of organic conductors have the composition of D_2X, where D is an organic donor molecule and X^- is a monovalent anion molecule. D_2X are synthesized by transferring an electron from the two donor molecules with closed shell to a counter anion molecule which becomes the monovalent anion molecules by taking an electron of the donor molecules, and have the closed shell. Among donor molecules, TMTSF and BEDT-TTF, which are shown in Fig. 1.1, are popular since their compounds $(TMTSF)_2X$ and $(BEDT\text{-}TTF)_2X$ exhibit the superconductivity [7, 8]. The donor and monovalent anion molecules compose 1D stacks or 2D layers depending on the donor molecules, and they stack alternately. The donor layers have 1/4 filling hole band since the two donor molecules with closed shell lose one electron by charge transfer to a counter anion, and the anion molecules are constructed of the insulating layers. The unit cell volume of organic conductors is about 1000 times as large as that of monoatomic metals since the composing elements of the organic conductors, i.e. the donor and anion molecules, are much larger than an atom. Therefore, the carrier density of them is too lower to screen the Coulomb interaction.

Organic conductors are regarded as a strongly correlated electron system since the Coulomb interaction is comparable to the transfer integral t. Typical values of t and the on-site Coulomb interaction U are 0.1 eV and 0.7 eV, respectively [9]. Some of κ-$(BEDT\text{-}TTF)_2X$, of which conduction band is 1/2 filling by the strong dimerization between BEDT-TTF molecules, are Mott insulators due to the large U. Moreover, organic conductors have the substantial off-site Coulomb interaction V as well as U. Typical value of V ranges from 0.2 to 0.35 eV. Electrons in organic conductors have a tendency to be localized due to the strong Coulomb interaction.

In some of them, the charge ordering state, which is an electron localized state due to the long range Coulomb interaction, is confirmed experimentally. The charge ordering state is mentioned in following section.

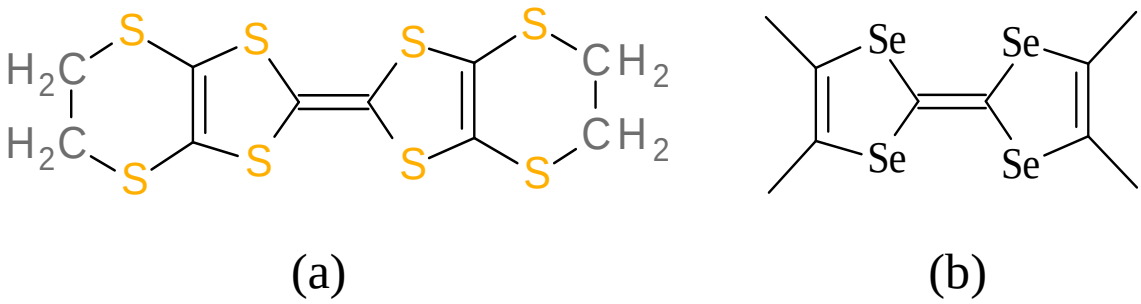

Figure 1.1: Structural formula of (a) BEDT-TTF and (b) TMTSF.

1.3 Charge order and charge disproportionation

1.3.1 Charge order

Charge order is an electron state in which electrons are localized due to the Coulomb interaction between electrons on the neighboring sites. Charge ordering phase has also been reported in the vicinity of the superconducting state [10, 11, 12] as shown in Fig. 1.2. Recently, charge ordering state has been attracted much attention from the standpoint of not only Wigner crystal in bulk, but also the superconductivity originates from charge fluctuation [13]. The electron system is described by the Hubbard Hamiltonian added the Coulomb interaction between electrons on neighboring sites, which is called the "extended Hubbard Hamiltonian" [9]. The extended Hubbard Hamiltonian is described as

$$H = \sum_{\langle i,j \rangle} \sum_{\sigma} \left(t_{i,j} a^{\dagger}_{i\sigma} a_{j\sigma} + \text{h.c.} \right) + \sum_{i} U n_{i\uparrow} n_{i\downarrow} + \sum_{\langle i,j \rangle} V_{i,j} n_i n_j. \tag{1.4}$$

where $t_{i,j}$ is the transfer integral between i-th and j-th site, U is the Coulomb interaction between electrons on a site, V is the Coulomb interaction between electrons on i-th site and j-th site. U and V are often called as the on-site and the off-site (long range) Coulomb interaction, respectively. If $U = \infty$, the spin degree of freedom can be neglected since double occupancy is prohibited. Taking into account the condition with $U = \infty$, the

above Hamiltonian is written as

$$H = \sum_{\langle i,j \rangle} \left(t_{i,j} a_i^\dagger a_j + \text{h.c.} \right) + \sum_{\langle i,j \rangle} V_{i,j} n_i n_j. \tag{1.5}$$

Now we consider the strongly correlated 1D electron system with 1/4 filling band by the extended Hubbard Hamiltonian with $U = \infty$. If $V > t$, electrons are arranged alternately on the 1D sites to reduce the Coulomb energy since two sites have one electron averagely in 1/4 filling. This is the charge ordering state. A schema of charge ordering state is depicted in Fig. 1.3.

The charge ordering state in quasi 1D system was reported below 220 K in an organic compound (DI-CNQI)$_2$Ag, where DI-DCNQI is diiodo-dicyanoquinonediimine, by ^{13}C-NMR measurement [14]. (DI-DCNQI)$_2$Ag has one dimensional chains of DI-DCNQI molecules in which overlaps of π-orbitals form quasi-one dimensional band. The ^{13}C-NMR measurement was reported to appear two DCNQI molecules with different electron density near the Fermi level below charge ordering transition temperature $T_{\rm CO}$ via Pauli magnetism on a DCNQI molecule. Moreover, the charge ordering state was reported in (TMTTF)$_2$X with quasi 1D system, where TMTTF is tetramethyltetrathiafulvalene and X is a monovalent counter anion [15]. Magnetic susceptibility has reported the Bonner-Fisher type temperature dependence which is explained by the Heisenberg model with an antiferromagnetic interaction, and the spin-Peierls state in the vicinity of the charge ordering state [16]. The behavior of magnetic susceptibility is explained by a presence of the antiferromagnetic interaction $J = t^2/U$ due to finite U.

Charge ordering state in quasi 2D system was reported in (BEDT-TTF)$_2$X with α- and θ- type BEDT-TTF donor, where BEDT-TTF is bis(ethylene)dithio-tetrathiafulvalene. Typical compounds exhibiting two dimensional charge ordering state are α-(BEDT-TTF)$_2$I$_3$ with $T_{\rm CO} = 135$ K [17, 18, 19] and θ-(BEDT-TTF)$_2$RbZn(SCN)$_4$ with $T_{\rm CO} = 195$ K [5]. In 2D charge ordering state, three kinds of charge stripe structures are predicted by the mean field calculation, in which the anisotropy of transfer integrals and the strength of the Coulomb interaction originates from BEDT-TTF molecule arrangemnt are taken account [9]. Figure 1.6 shows the stripe structures. The stripe structures are defined by the direction, along which charge aligns, to linear alignment of the molecules (column). The charge stripe, in which charge alignment is perpendicular to the column as shown in Fig, 1.6 (a),

is the horizontal stripe, and that with charge alignment parallel to the column is vertical one as shown in Fig. 1.6 (b). The mean filed calculation suggested that horizontal and vertical charge stripes are plausible in $\alpha-$ and $\theta-$ type BEDT-TTF compounds. Horizontal stripe structure was found in α-(BEDT-TTF)$_2$I$_3$ and θ-(BEDT-TTF)$_2$RbZn(SCN)$_4$ by ^{13}C-NMR [17], X-ray diffraction [18] and infrared reflectivity [19].

At the charge ordering transition in quasi two-dimensional electronic systems, it has been observed by Raman spectroscopy, X-ray diffraction measurement that the structural change occurs accompanying with the development of the charge structure [20, 21]. Especially, in θ-(BEDT-TTF)$_2$RbZn(SCN)$_4$, the large rearrangement has been reported by X-ray diffraction [20]. In the rearrangement, neighboring BEDT-TTF molecules along the column dimerize in such a way as to appear the ferroelectricity. The correlation length of the rearrangement depends on the cooling speed across the transition temperature. When cooling rate is less than 0.2 K/min around $T_{\rm CO}$, the coherence length is on a long scale. In the case with more rapid cooling than 5 K/min, the diffuse spots $\boldsymbol{q} = (1/3\ k\ 1/4)$, which corresponds to charge disproportionation on donor arrangement with absence of the dimerization above $T_{\rm CO}$, still remain below $T_{\rm CO}$. Therefore, the correlation length is expected to be shorter than the case of slow cooling rate 0.2 K/min. It was reported that $T_{\rm CO}$ also depends on the cooling rate by temperature dependence of permittivity [22]. With cooling rate of 0.1 K/min, an spike like anomaly of permittivity corresponding to charge ordering transition has been observed around $T_{\rm CO} = 195$ K. Temperature of the anomaly decreases with increasing the cooling rate, and then the spike like anomaly is completely suppressed above cooling rate of 9 K/min. Pump probe spectroscopy reported that the recovery time of charge ordering state in θ-(BEDT-TTF)$_2$RbZn(SCN)$_4$ is shorter than that in α-(BEDT-TTF)$_2$I$_3$ of which rearrangement of BEDT-TTF molecules accompanied with charge ordering transition is smaller than that of θ-(BEDT-TTF)$_2$RbZn(SCN)$_4$ [23]. Therefore, on charge ordering transition in quasi 2D electron system, V do not only play a important role, but also electron-phonon interaction. The charge ordering state is not "Wigner crystal on lattice" exactly although it is "Wigner crystal on lattice" like.

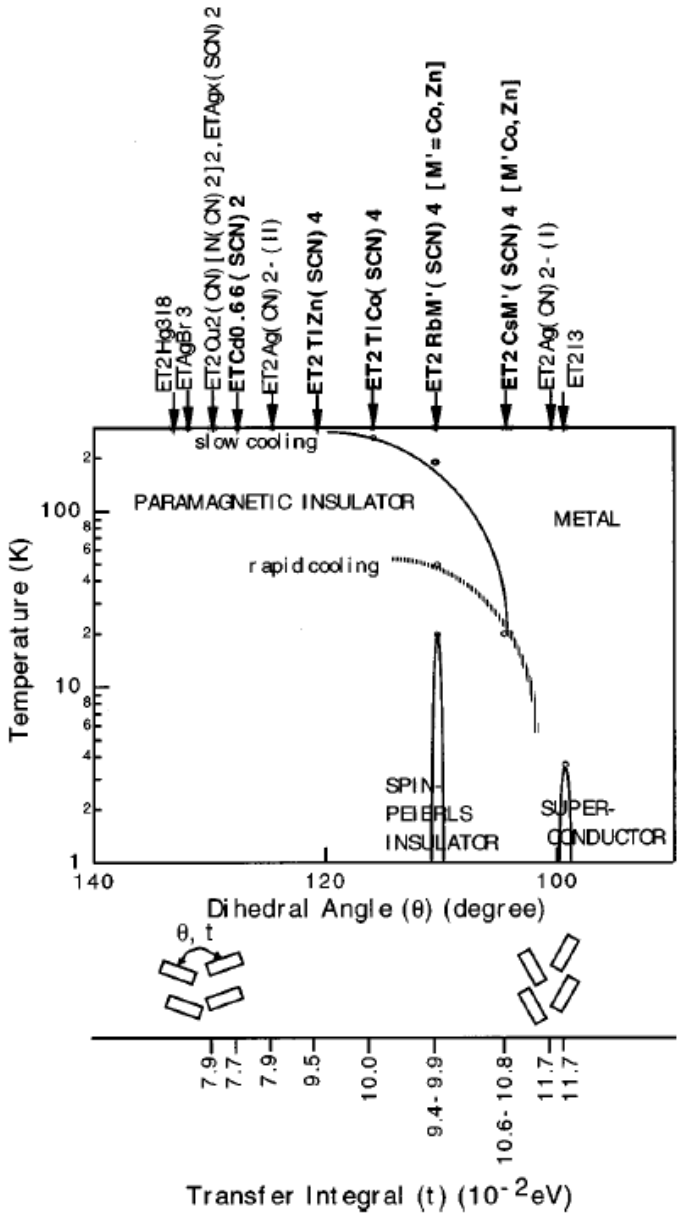

Figure 1.2: Phase diagram of θ-type BEDT-TTF compounds as a function of dihedral angle [11]. The transfer integral increases with increasing the dihedral angle since overlap between π-orbitals around sulfur atoms of neighboring BEDT-TTFs increase, which are expanded perpendicular to molecular plane of the BEDT-TTF.

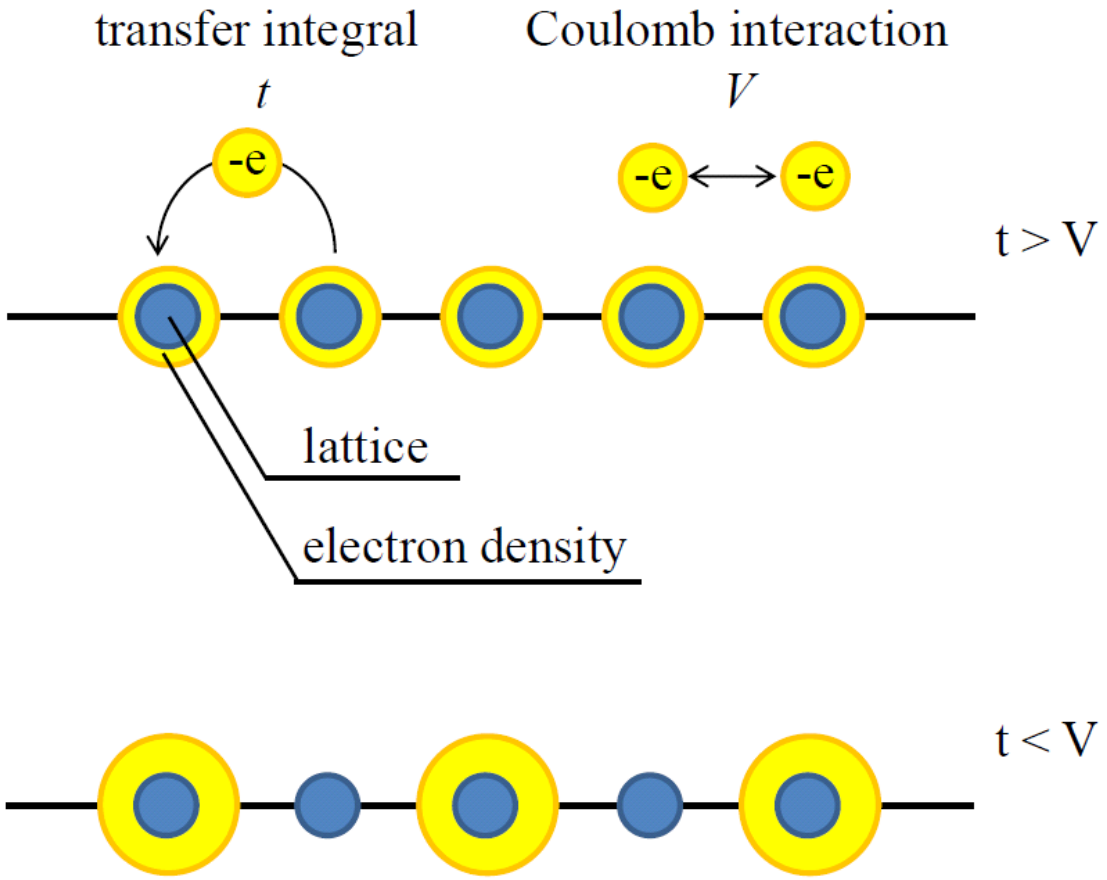

Figure 1.3: Schema of charge distribution in one dimensional chane under (a) $t > V$ and $t > V$, where t is transfer integral and V is Coulomb interaction between electrons on neighboring sites. Under the condition (a), electrons spread to gain kinetic energy. On the other hand, under the condition (b), electrons localize at alternate sites to reduce the Coulomb energy.

1.3.2 Charge disproportionation

As mentioned above, charge disproportionation has been observed even above T_{CO} in θ-(BEDT-TTF)$_2$RbZn(SCN)$_4$ and α-(BEDT-TTF)$_2$I$_3$ [17, 18, 20, 22]. In θ-(BEDT-TTF)$_2$ RbZn(SCN)$_4$, the diffuse of $\boldsymbol{q} = (1/3\ k\ 1/4)$ corresponding to charge disproportionation was observed above T_{CO} [48]. The charge disproportionation is replaced by horizontal stripe structure with which structural change is on a long scale when cooling rate is less than 0.2 K/min. In the case with more rapid cooling than 5 K/min, the charge disproportionation still remains below T_{CO}. In α-(BEDT-TTF)$_2$I$_3$, the charge disproportionation

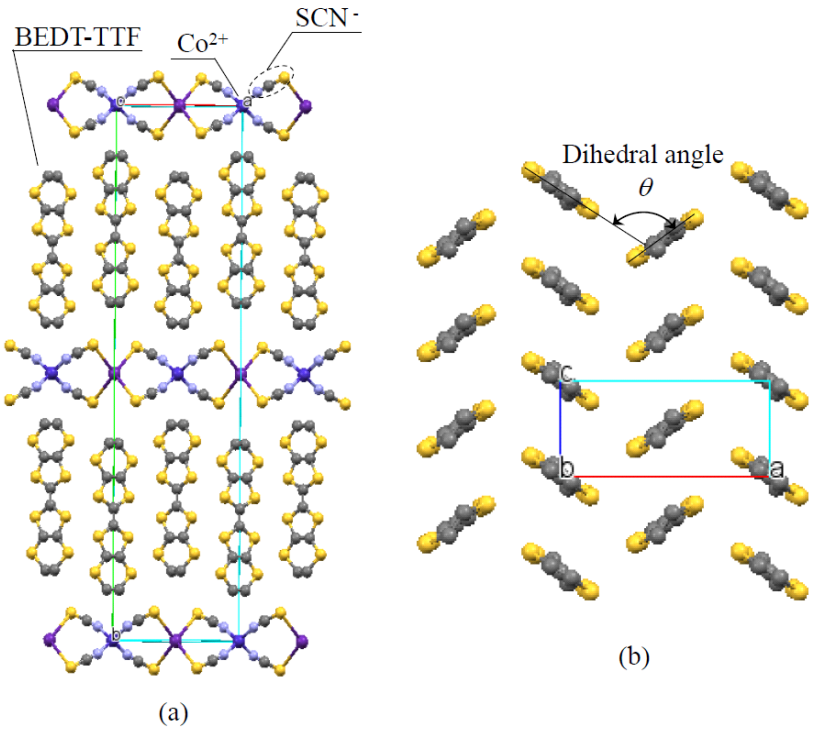

Figure 1.4: Crystal structure of θ-(BEDT-TTF)$_2$RbCo(SCN)$_4$ along (a) c^* direction and (b) b^* direction. You can get crystal structure of θ-(BEDT-TTF)$_2$RbZn(SCN)$_4$ by replacing Co^{2+} in the figure with Zn^{2+}. Space group of the structure is I222. A BEDT-TTF is on the two fold axis, Rb^+ and Co^{2+} are located on cross point of the two fold axes. So, There is just one crystallographically BEDT-TTF molecule in the unit cell.

among A, B and C BEDT-TTF molecules was reported far above T_{CO} [18]. The ratio of charge disproportionation of B and C BEDT-TTF molecules develops with decreasing temperature. The charge disproportionation is also expected to be due to the long-range Coulomb interaction similarly to the charge ordering state since the Coulomb interaction does not depend on temperature in the temperature region up to room temperature. Moreover, the charge disproportionation state is more "Wigner crystal on lattice" like than charge ordering state, since the rearrangement of BEDT-TTF molecules does not occur.

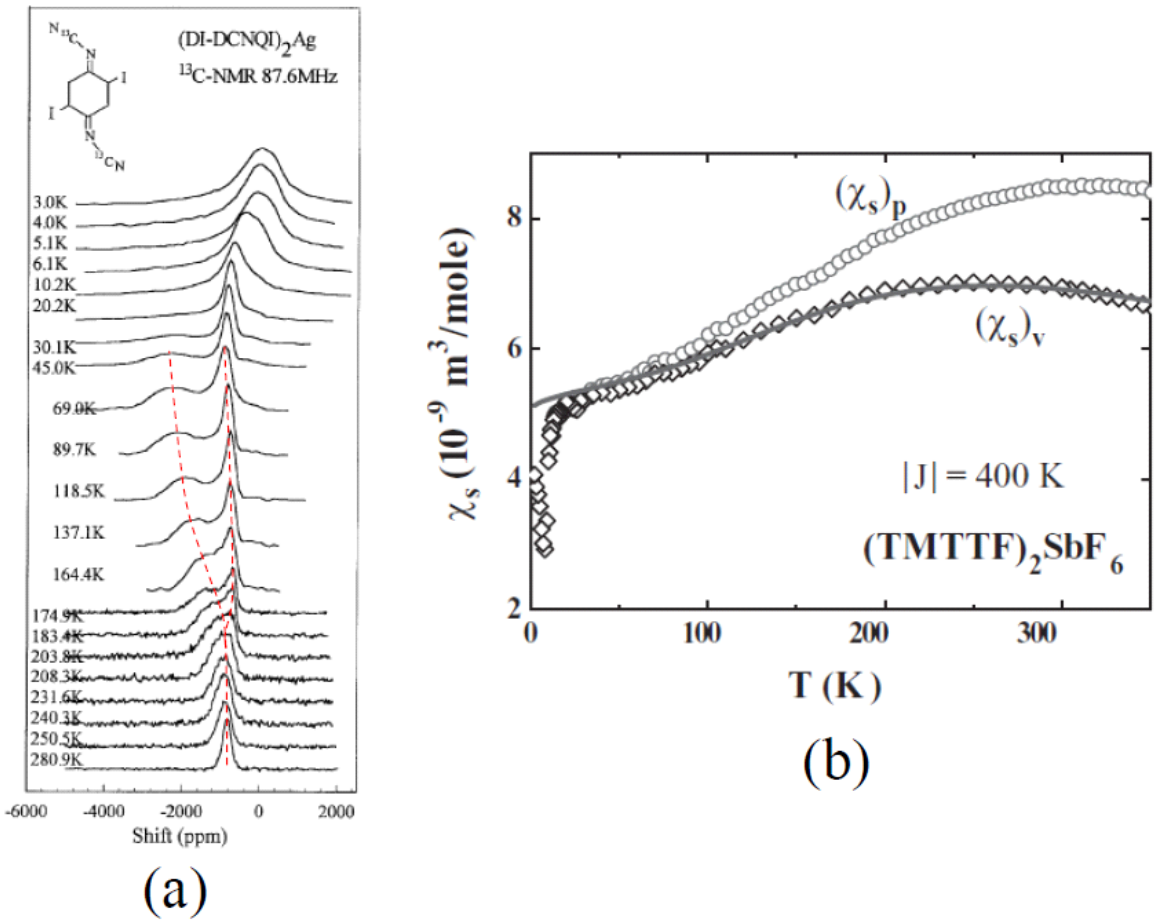

Figure 1.5: (a) ^{13}C-NMR spectra of (DI-DCNQI)$_2$Ag at various temperature [14]. T_{CO} of (DI-DCNQI)$_2$Ag is 220 K. Red break line indicate center of peaks of the spectra continuously. (b) Temperature dependence of magnetic susceptibility of (TMTTF)$_2$SbF$_6$ at constant pressure $(\chi_{\mathrm{s}})_p$ (circles) and at constant volume $(\chi_{\mathrm{s}})_V$ (diamonds) [16]. T_{CO} of (TMTTF)$_2$SbF$_6$ is 157 K.

1.4 Purpose of this study

Wigner crystal appears in various situation such as white dwarfs in universe [25], inversion layer on interface of GaAs/GaAlAs under strong magnetic field [26, 27, 28, 29]. Also since localized states due to the long-rage Coulomb interaction such as Mott insulator and charge order appear in the vicinity of the superconducting state, it is very important to understand the role of the Coulomb interaction as the long range interaction in strongly

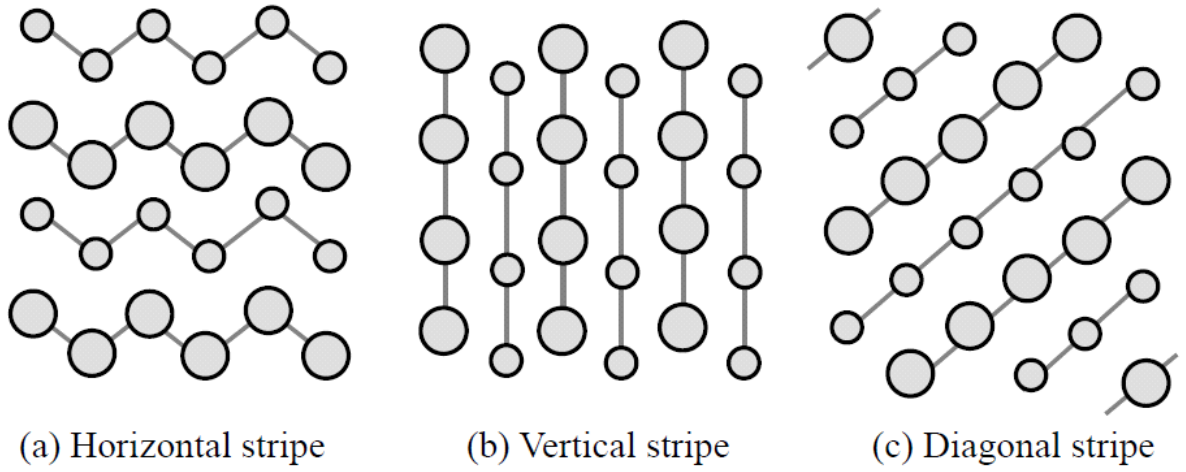

Figure 1.6: The schema of the three types of charge order; (a) horizontal stripe, (b) vertical stripe, and (c) diagonal stripe. The circles represent the BEDT-TTF molecules and their diameters express the charge amount on the BEDT-TTF molecules. The arrow in left side of the figure indicates direction of the columns of the BEDT-TTF molecules.

correlated system. However, since the particle arrangement in Winger crystals has not been directly observed yet in the real space, domain boundary and the structure of charged particles in Wigner crystals have not been understood yet.

Then we clarify the relation of the long range Coulomb interaction and the structure of charged particles, and electronic state near the domain boundary by performing scanning tunneling microscopy (STM) on the charge disproportionation state.

As mentioned above, the charge disproportionation is not affected by the rearrangement of BEDT-TTF. Besides it is easy to control the distance between electrons and realize anisotropic system by replacing the anion of charge disproportionation compound with different shape. It is expected to be able to observe charge structure since the arrangement of organic molecules in an organic conductor TTF-TCNQ has been observed by scanning tunneling microscopy [32].

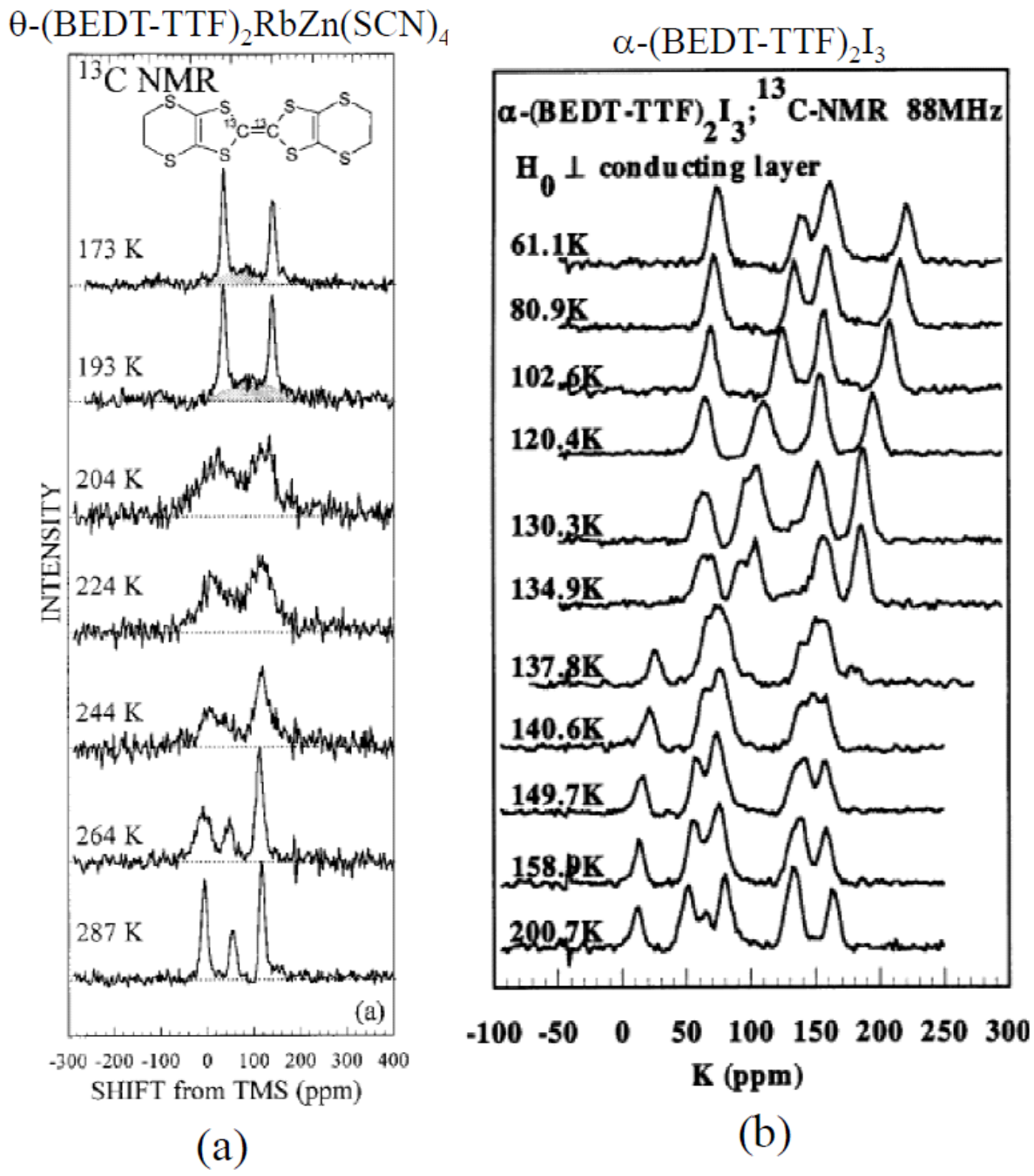

Figure 1.7: ^{13}C-NMR spectra of (a) θ-(BEDT-TTF)$_2$RbZn(SCN)$_4$ [5] and (b) α-(BEDT-TTF)$_2$I$_3$ [30] at various temperature. $T_{\rm CO}$ of θ-(BEDT-TTF)$_2$RbZn(SCN)$_4$ and α-(BEDT-TTF)$_2$I$_3$ are 195 K and 135 K, respectively. In these measurements, ^{13}C atoms were enriched at two carbon sites at center of a BEDT-TTF since the carbon sites have large electron density.

1.5 Physsical properties of α-(BEDT-TTF)$_2$X

1.5.1 Donor arrangement with α-type

α-(BEDT-TTF)$_2$I$_3$ has a layered structure. Metallic BEDT-TTF and insulating I_3^- layers are alternatively stacked along the c-axis. Figure 1.10 shows the BEDT-TTF donor layer of α-(BEDT-TTF)$_2$I$_3$ as an example. A rectangle in Fig. 1.10 represents the unit cell of BEDT-TTF molecules arrangement with α-type. The BEDT-TTF molecules in a layer are placed at the same position along the direction stacking BEDT-TTF and insulating layers. There are two types of donor stacking columns, which are denoted by I and II, along the a-axis. The unit cell contains four BEDT-TTF molecules, A, A', B, and C. The column I consists of A and A', and the column II consists of B and C. It should be noted that A and A' are crystallographically equivalent, and B and C are independent. In this study, α-(BEDT-TTF)$_2$I$_3$ and α-(BEDT-TTF)$_2$MHg(SCN)$_4$ are chosen to exclude the effect of height variation on surface.

1.5.2 α-(BEDT-TTF)$_2$I$_3$

The crystal structure of α-(BEDT-TTF)$_2$I$_3$ is triclinic with space groupe of $P\bar{1}$. Lattice parameters are a = 0.9187 nm, b = 1.0793 nm, c = 1.7400 nm, α = 96.536 °, β = 97,911 °, γ = 90.795 ° at room temperature [33]. The donor arrangement is α-type as shown in Fig. 1.10. At room temperature, only A and A' molecules along column I are dimerized. The resistivity decreases with decreasing temperature and increases drastically below charge ordering transition temperature T_{CO} = 135 K [34]. The charge structure of charge ordering state is horizontal type structure in which A and B molecules are charge rich, and other molecules are poor [17, 19, 33]. It has been reported that the B and C molecules along column II were dimerized in the charge ordering state. The displacements of each molecules evaluated from X-ray diffraction pattern are shown Table 1.1.

Above T_{CO}, charge disproportionation has been reported from X-ray [33] diffraction, raman spectroscopy [19] and ^{13}C-NMR [17]. The ratio of the disproportionation between B and C molecules develops with decreasing temperature.

Table 1.1: The table summarizing the molecule displacement at the charge ordering transition. $*$ 1 and $*$2 means that it is unable to detect precisely and almost zero.

molecule	$\Delta a/a \times 10^{-4}$	$\Delta b/b \times 10^{-4}$	$\Delta c/c \times 10^{-4}$
BEDT "A"	$*$ 1	0	$*$ 1
BEDT "B"	45	0	$*$ 2
BEDT "C"	-45	0	$*$ 2
I_3 "D"	-15	0	-11
I_3 "D"	15	0	11

1.5.3 α-(BEDT-TTF)$_2$MHg(SCN)$_4$

The crystal structure of α-(BEDT-TTF)$_2$KHg(SCN)$_4$ is triclinic with space group of $P\bar{1}$. Lattice parameters are a = 1.0018 nm, b = 2.0586 nm, c = 0.9921 nm, α = 103.62 °, β = 90.45 °, γ = 93.31 ° at room temperature. That of α-(BEDT-TTF)$_2$RbHg(SCN)$_4$ is triclinic space group $P\bar{1}$ with lattice parameters a = 1.0061 nm, b = 2.0602 nm, c = 0.9976 nm, α = 103.70 °, β = 90.58 °, γ = 93.19 ° at room temperature [36]. They have almost the same crystal structure. Their anion layer consists of a sheet with K^+ and Hg^{2+} sandwiched between two sheets with SCN^-, so it is thicker than the anion layer of α-(BEDT-TTF)$_2$I$_3$.

Fermi surfaces of α-(BEDT-TTF)$_2$MHg(SCN)$_4$ consist of two sheet like ones and one cylindrical one, which are different with that of α-(BEDT-TTF)$_2$I$_3$ [37]. At low temperature, the density wave transition was reported due to the nesting between two sheet like Fermi surfaces, where T_{DW}s of M = K, Rb are 8 and 12 K, respectively [38].

1.6 Scanning tunneling microscopy

Scanning tunneling microscopy (STM) is a powerful tool to be able to probe local electron density in real space on the atomic scale, since its invention by G. Binnig and H. Rohrer in 1981 [39]. The high spatial resolution is due to the exponential dependence of tunneling current on the distance between STM tip and the sample surface. The tunneling current I is described with distance d as

$$I(\boldsymbol{r}) = I_0(\boldsymbol{r}) \exp(-\frac{2d(\boldsymbol{r})}{\lambda}) \tag{1.6}$$

with

$$\lambda = \sqrt{\frac{\hbar^2}{2m\phi}} \tag{1.7}$$

$$I_0(\boldsymbol{r}) = \int_{E_\mathrm{F}}^{E_\mathrm{F}+eV} N(E, \boldsymbol{r}) dE \tag{1.8}$$

where E_F is the Fermi energy, $N(E)$ is the local density of state at a position $\boldsymbol{r}$, λ is the decay length of tunneling current, V is bias voltage between STM tip and the sample, and ϕ is the work function of sample. The typical value of the decay length is sub-angstrom order. Therefore, STM can probe variation of local electron density in real space with atomic scale since tunneling current only flow between top of the STM tip and the atom closest to it on the surface.

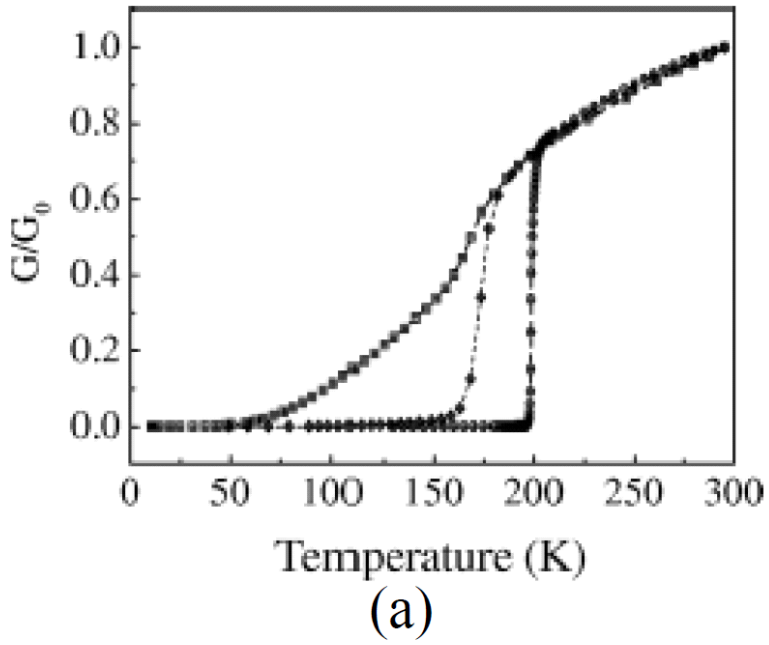

(a)

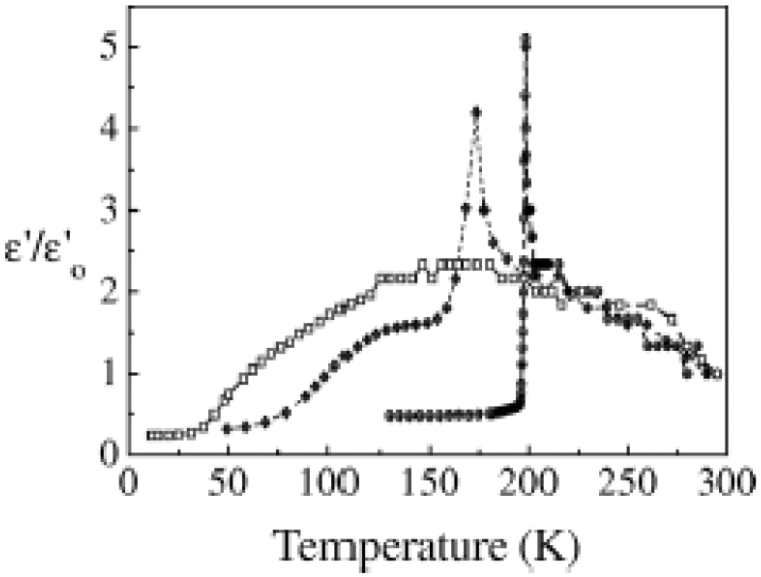

(b)

Figure 1.8: (a) Temperature dependence of conductance and dielectric permittivity normalized by their values at room temperature with three cooling rate. The data of the slow cooling at 0.1 K/min (relaxed state), intermediate cooling at 4 K/min(intermediate state) and fast cooling at 9 K/min (quenched state) are denoted by open circles, open diamonds and open squares, respectively. T_{CO} with slow cooling is 195 K [22].

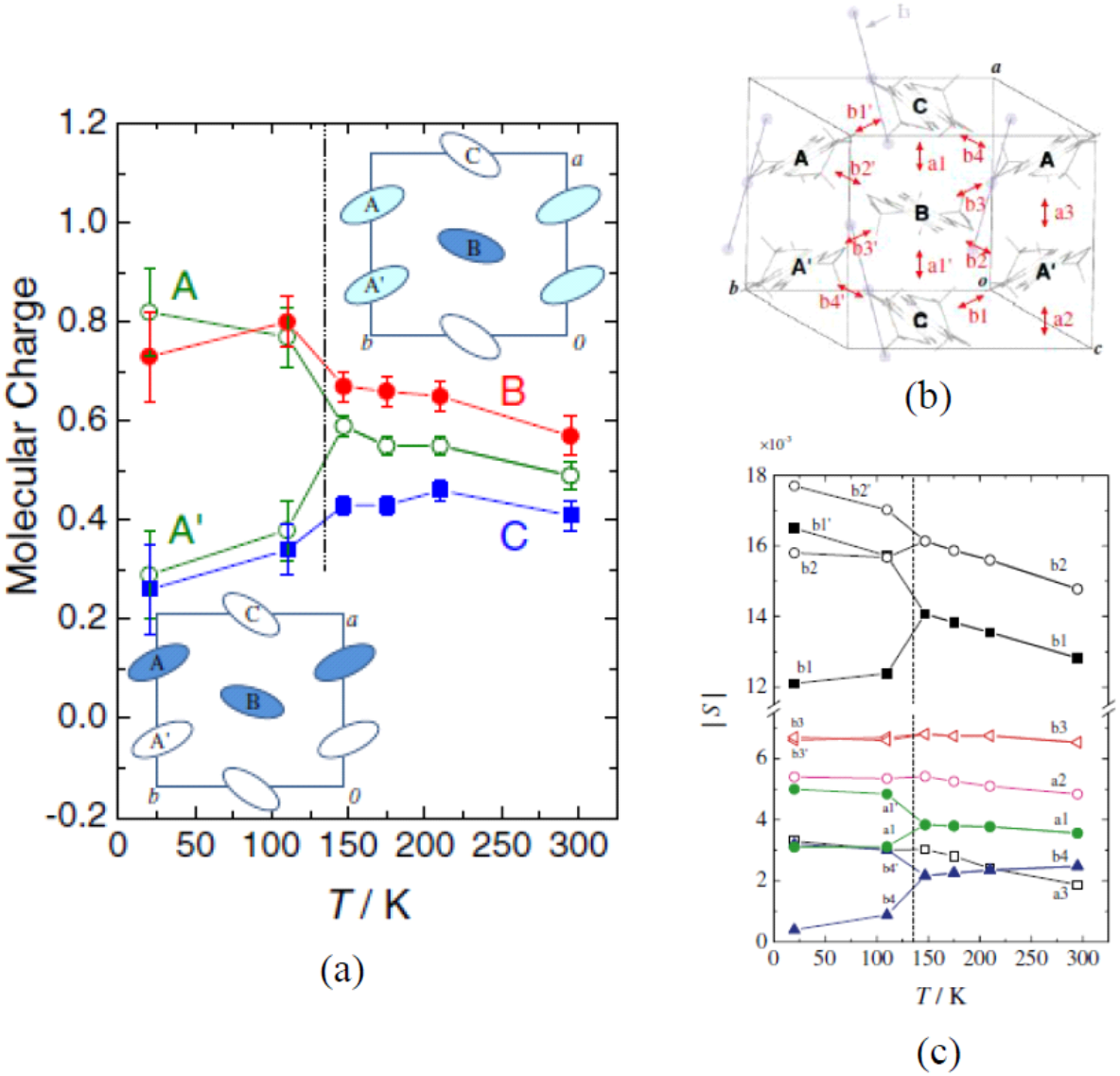

Figure 1.9: Temperature dependence of (a) charges on each BEDT-TTF molecules and transfer integrals (c) [18]. The amounts of charge on each BEDT-TTF and each transfer integrals are estimated by an empirical method based on bond lengths in the BEDT-TTF [31] and by extended Huckel method. The transfer integrals in (c) correspond to them in (b). BEDT-TTF B has larger amount of charge than BEDT-TTF C throughout entire temperature region. The donor arrangement with one kind of transfer integrals on Column II "a1" charges to that with two kinds of transfer integral on Column II, "a1" and "a1'" below $T_{CO} = 135$ K.

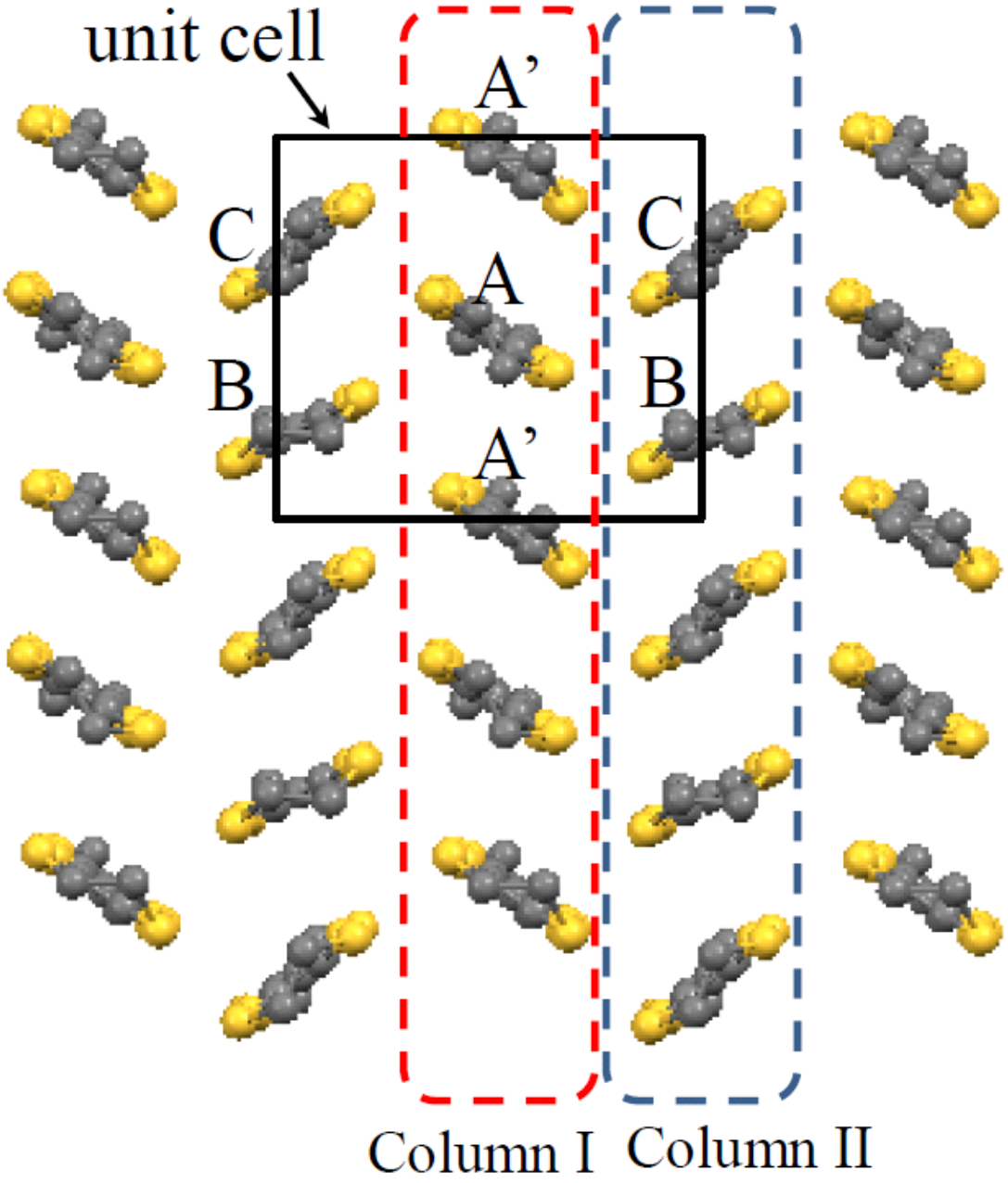

Figure 1.10: α-type BEDT-TTF arrangement. A unit cell of α-type arrangement consists of four molecules A, A', B and C, in which A, B and C are crystallographically equivalent and A and A' are equivalent. The inversion centers are located at the center of A and A' and on B and C. A and A' are weakly dimerized.

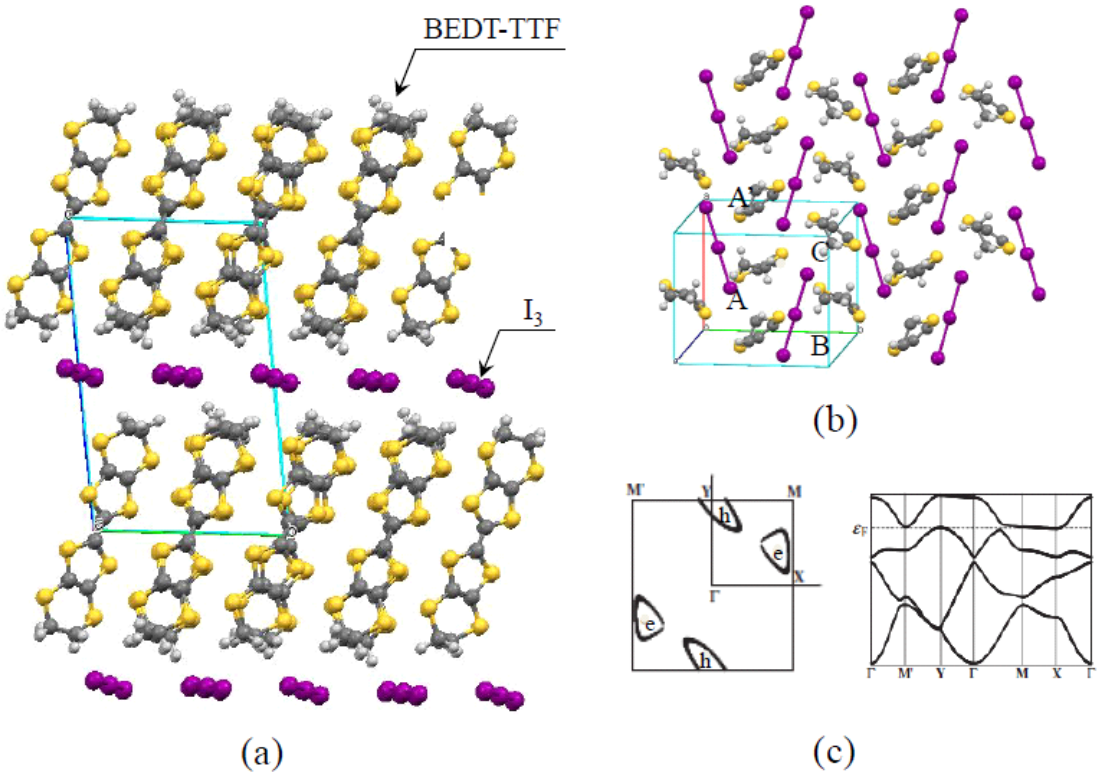

Figure 1.11: Crystal structures of α-(BEDT-TTF)$_2$I$_3$ along (a) a^* direction and (b) c^* direction, and Fermi surface and band structure of it (c) [35]. There are two hole pockets denoted by a character "h" and two electron pockets denoted by a character "e".

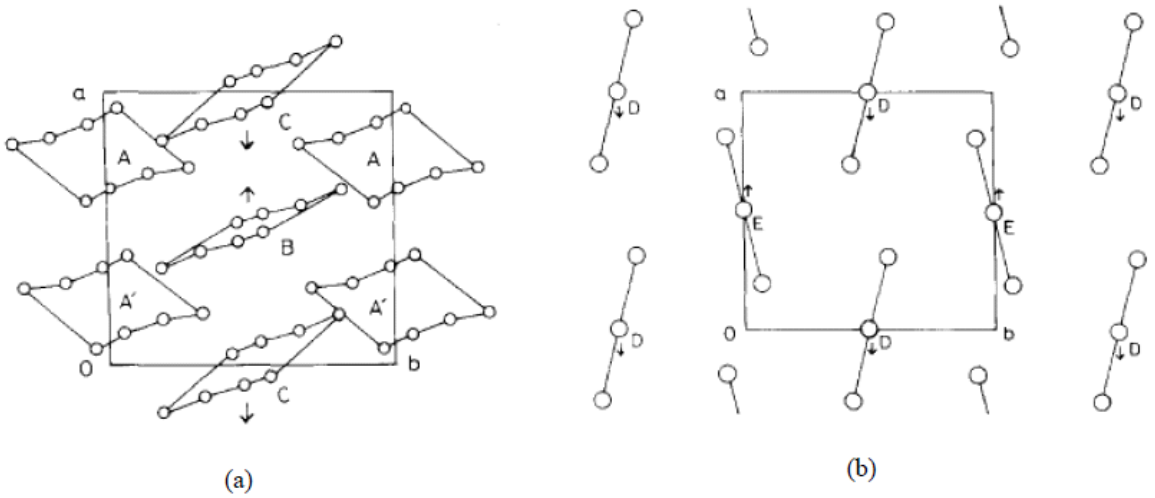

Figure 1.12: Schema of structural change on (a) a BEDT-TTF layer and (b) an anion layer at T_{CO} in α-(BEDT-TTF)$_2$I$_3$. In (a), only frames formed by sulfur atoms of the BEDT-TTFs are shown for the sake of simplicity. Potion of an unit cell in the anion layer corresponds to that in the BEDT-TTF layer. Arrows indicate the direction of the model displacement of BEDT-TTF molecules and I a anions, respectively [33]. The values of the displacements are shown in Table. 1.1

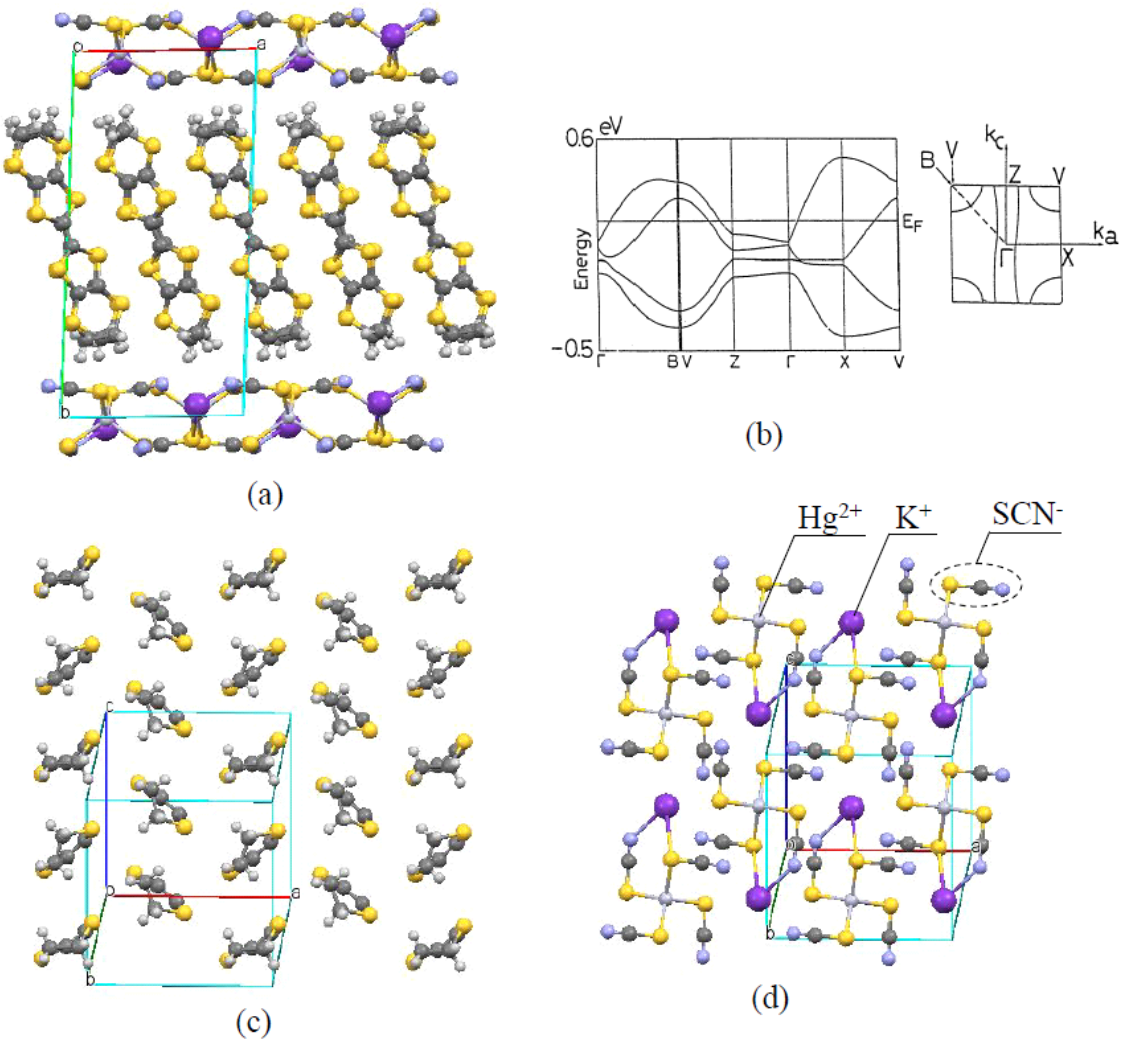

Figure 1.13: (a) Crystal structure of α-(BEDT-TTF)$_2$KHg(SCN)$_4$ along the c^* direction. One can get crystal structure of α-(BEDT-TTF)$_2$RbHg(SCN)$_4$ by replacing K^+ with Rb^+. (b) Band structure and Fermi surface of α-(BEDT-TTF)$_2$KHg(SCN)$_4$ [37]. Band structure and Fermi surface of α-(BEDT-TTF)$_2$RbHg(SCN)$_4$ are almost same as those of α-(BEDT-TTF)$_2$KHg(SCN)$_4$. Arrangement of (c) BEDT-TTFs and (d) anions. In (c), one-sides of outer ring of BEDT-TTFs are only shown fro simplicity. Balls with yellow, dark gray and light gray in SCN^- molecules are sulfur, carbon and nitrogen atoms, respectively.

Chapter 2

Experimental method

2.1 Samples

Single crystals of α-(BEDT-TTF)$_2$I$_3$ salt used in this study were synthesized by Dr. K. Yamamoto (Department of Applied Physics, Okayama University of Science). Single crystals of α-(BEDT-TTF)$_2$MHg(SCN)$_4$ (M = K, Rb) were synthesized by electro-chemical method with controlled applied current method. The applied current was increased along the curve derived from the equation, $I = ct^2$, where t is time, and c is a constant depending on the amount of solvents and the period of crystal growth.

The shape of the single crystals in this study is the thin rectangle with 1 mm $\times$ 1 mm $\times$ 0.1 mm. The largest surface of the single crystal is the conducting surface.

2.1.1 Ingredients of α-(BEDT-TTF)$_2$MHg(SCN)$_4$(M=K,Rb)

The reagents used in the synthesis of sample crystals are listed in Table. 2.2. 1,1,2-trichloroethane with guaranteed reagent (GR) grade made by Nacalai Tesque. Inc. was used as the solvent. Reagents were purified by recrystallization to prevent the impurities being mixed into the samples.

Table 2.1: The ingredients of α-(BEDT-TTF)$_2$KHg(SCN)$_4$

Ingredients	Actual producer	solute(amount)	number of mol
BEDT-TTF [Mw = 384.72]	Tokyo Chemical Industry CO. (Recrystalization)	81.7 mg	212 mmol
Hg(SCN)$_2$ [Mw = 316.78]	Wako Pure Chemical Industries, Ltd.	95.7 mg	302 mmol
KSCN [Mw = 97.01]	Wako Pure Chemical Industries, Ltd.	61.0 mg	629 mmol
18-crown-6 ether [Mw = 264.32]	Wako Pure Chemical Industries, Ltd.	159.3 mg	603 mmol
1,1,2-Trichloroethane	Nacalai Tesque. Inc.	180 ml	
Ethanol	Wako Pure Chemical Industries, Ltd.	20 ml	

Table 2.2: The ingredients of α-(BEDT-TTF)$_2$RbHg(SCN)$_4$

Ingredients	Actual producer	mass (amount)	number of mol
BEDT-TTF [Mw = 384.72]	Tokyo Chemical Industry CO. (Recrystalization)	81.7 mg	212 mmol
Hg(SCN)$_2$ [Mw = 316.78]	Wako Pure Chemical Industries, Ltd.	76.8 mg	242 mmol
RbSCN [Mw = 143.56]	Wako Pure Chemical Industries, Ltd.	98.5 mg	686 mmol
18-crown-6 ether [Mw = 264.32]	Wako Pure Chemical Industries, Ltd.	164.5 mg	622 mmol
1,1,2-Trichloroethane	Nacalai Tesque. Inc.	200 ml	
Ethanol	Wako Pure Chemical Industries, Ltd.	22 ml	

2.1.2 Crystal growth of α-(BEDT-TTF)$_2$MHg(SCN)$_4$ (M = K, Rb)

Single crystals were grown by the electro-chemical oxicidation of BEDT-TTF in 1,1,2-trichloroethane containing KSCN (RbSCN), $Hg(SCN)_2$ and 18-crown-6 ether. The experimental instruments used in this process were cleaned with pure water, and were dried in the oven at 120 °C for a day to prevent some impurities being mix into the samples.

The single crystals were grown in argon gas atmosphere with ambient pressure at room temperature. Conical flask connected to the test tube by two narrow glass tubes were used as crystal growth cells. Crystals were grown in conical flasks of crystal growth cells. The applied current was changed discontinuously from 0.5 to 6 μA along the curve derived from the equation, $I = ct^2$. The period growing the single crystals was about 1 month.

2.1.3 Sample characterization

The electronic property of grown single crystals was characterized by the static magnetic susceptibility measurement with SQUID magnetometer.

In the magnetic susceptibility measurement, single crystals were packed by a thin film of kapton whose masses were 16.8 mg and 8.8 mg, respectively. The amount of the sample were adjusted in such a way that magnetization is less than about 10 % of that of sample. Masses of K and Rb salts were 41.2 mg and 13.6 mg, respectively Large amount of K salt were used to observe a small reduction of the magnetic susceptibility at the density wave transition T_{DW}. The magnetization was measured with applying magnetic field of 1 T.

Figure 2.1 and 2.2 show the temperature dependence of the magnetic susceptibility of K and Rb salts, respectively. Magnetic susceptibility of the sample is evaluated by subtracting the susceptibility of the kapton sheet measured individually. The decrease of the magnetic susceptibility in K and Rb salts was observed at 7.2 K and 12 K, respectively, which corresponds to T_{DW}. The decreases is explained by a reduction of the Pauli paramagnetism due to the density wave transition. Curie tail by impurity was observed below 5 K in both K and Rb salts. The amount of impurities evaluated from the Curie component is less than 8 per 1000 BEDT-TTF sites in both K and Rb salts.

Therefore, we could get single crystals with high quality of both K and Rb salts in this study.

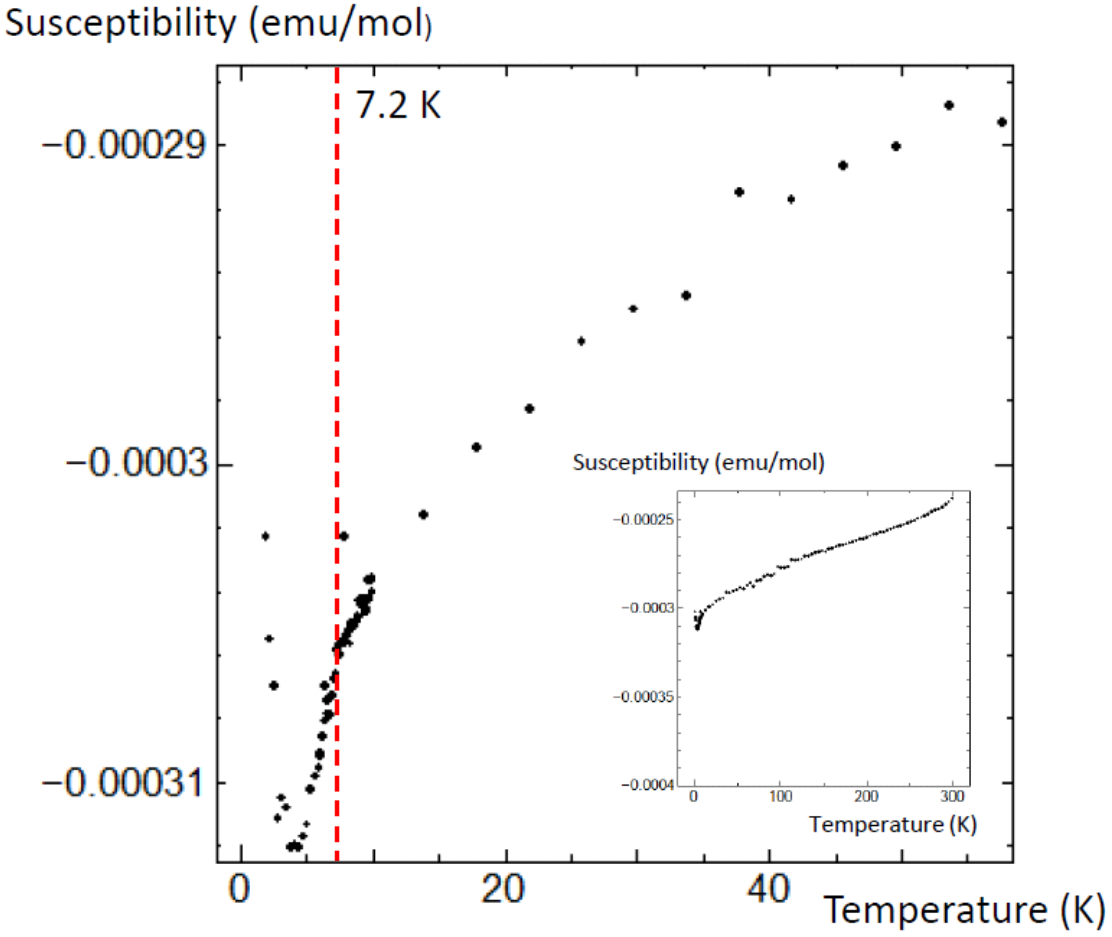

Figure 2.1: Temperature dependence of magnetic susceptibility of α-(BEDT-TTF)$_2$KHg(SCN)$_4$. Density wave transition temperature T_{DW} is indicated by red broken line.

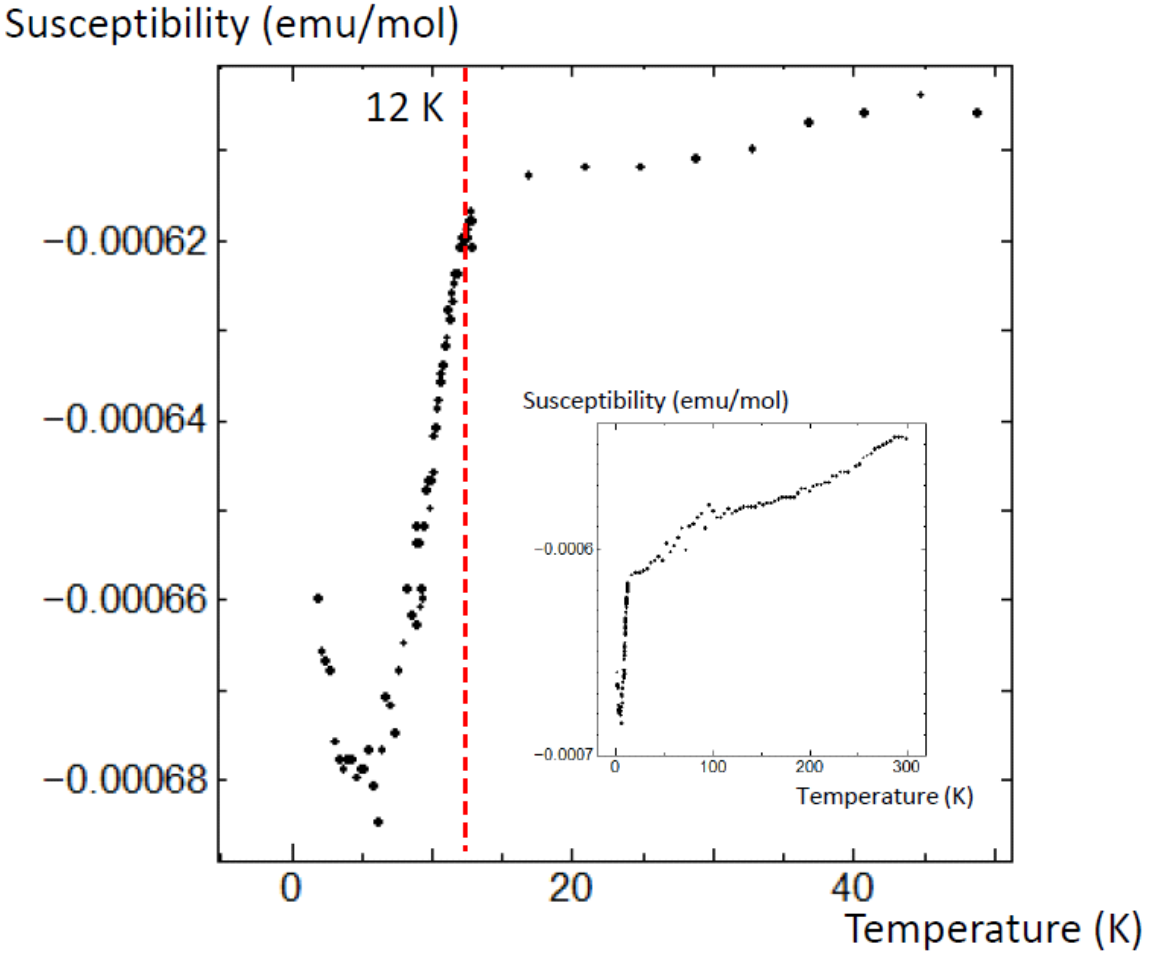

Figure 2.2: Temperature dependence of magnetic susceptibility of α-(BEDT-TTF)$_2$RbHg(SCN)$_4$. Density wave transition temperature T_{DW} is indicated by red broken line.

2.2 Sample setting and scanning tunneling microscopy

Figure 2.3 shows the schema of sample setting. Single crystals were glued by carbon paste on the phosphor bronze plate. The phosphor bronze plate was mounted on the STM sample stage with Apiezon grease N. The phosphor bronze plate was connected by a silver wire of 5 μm in diameter in order to make it connect to STM sample stage electrically. STM observation was performed on shiny areas of the surface which was not especially treated for STM observation.

The commercial scanning tunneling microscopy made in JEOL was used. Pt-Ir wires were used as STM tips by cutting with a nipper. The STM tips used in this study were confirm to have atomic resolution by observing atom arrangement of graphite, before the measurement. Figure 2.4 shows a typical STM image of graphite.

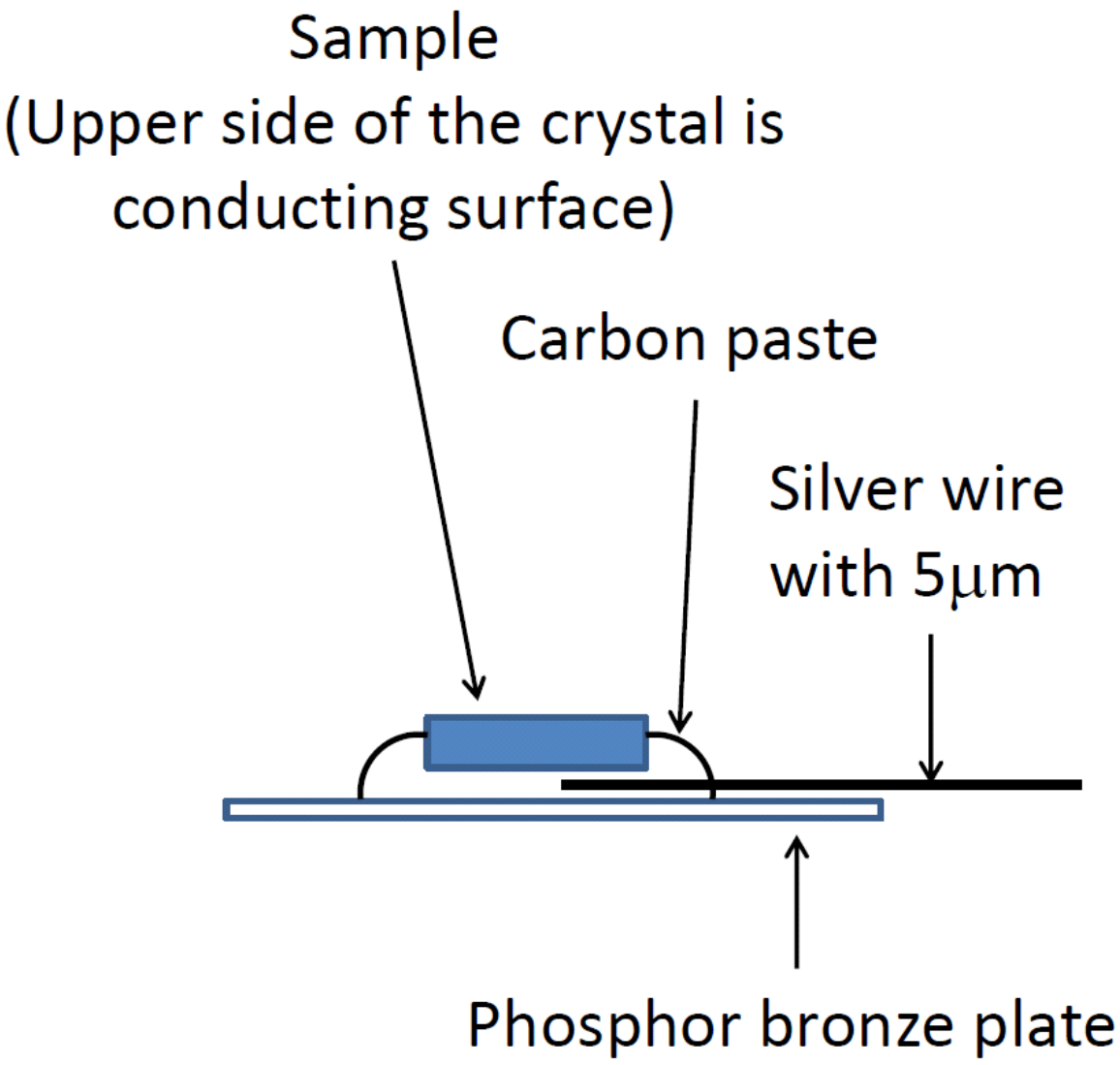

Figure 2.3: The schema depicting the sample preparation for STM measurement.

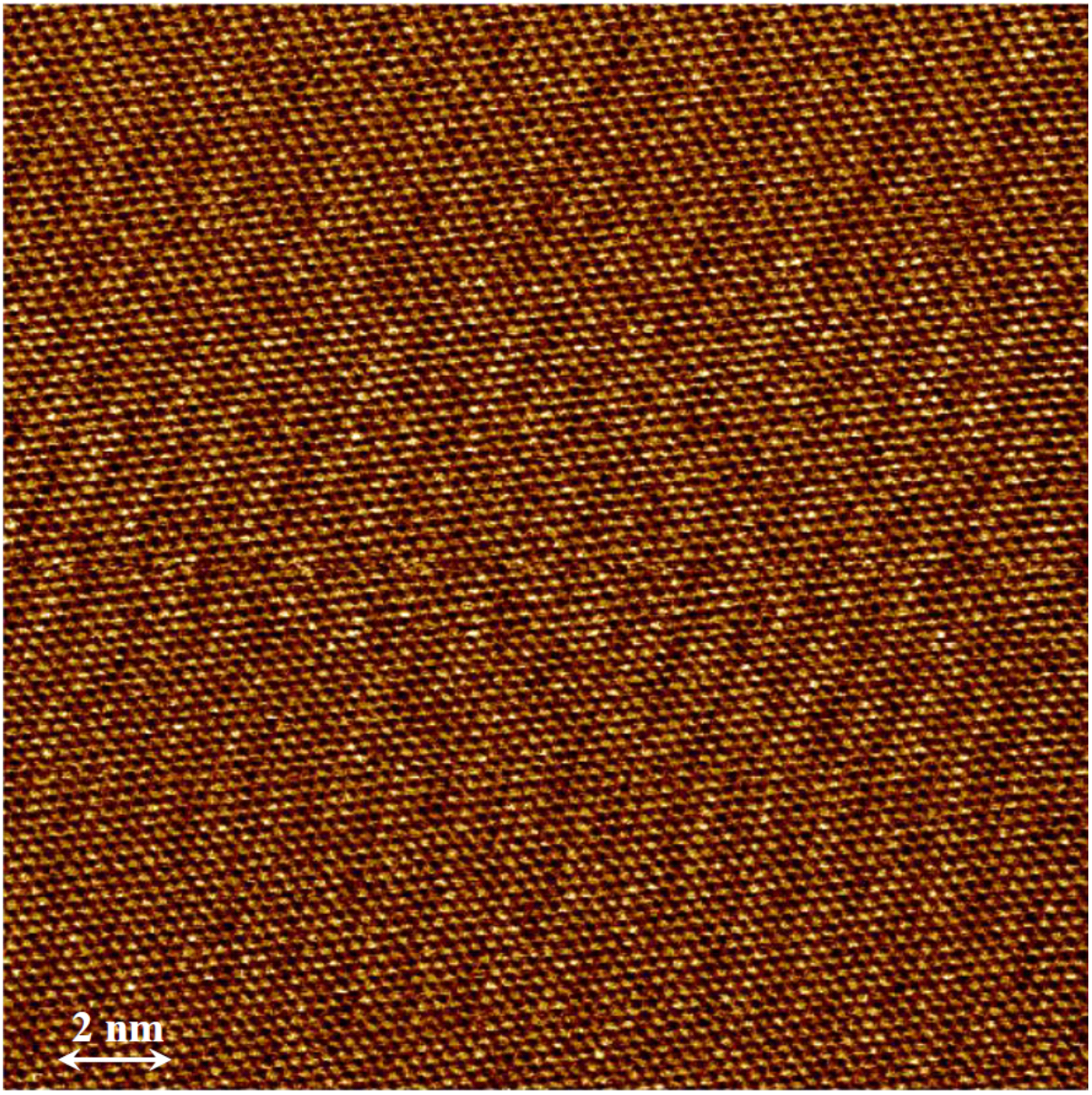

Figure 2.4: STM current image of the graphite.

Chapter 3

Results

3.1 α-(BEDT-TTF)$_2$I$_3$

3.1.1 Charge distribution

Figure 3.1 shows the STM current image on the $a-b$ plane with the bias voltage $V = 50$ mV and the tunneling current $I = 50$ pA. The scanning area is 9.4×6.2 nm^2. BEDT-TTF molecules were clearly imaged as ellipse spots. The face centered rectangle pattern was clearly observed. The pattern corresponds to α-type donor arrangement. The periodicity of spots is consistent with lattice parameters, $a = 0.9187$ nm and $b = 1.0793$ nm of α-(BEDT-TTF)$_2$I$_3$. The a and b-directions are assigned as indicated in Fig. 3.1. From the shape of spots, the slant alternation was found along the b-axis. Then we can distinguish column I and II.

It was observed that the intensity varies depending on the donor site. The tunneling current depends on both the electronic density of states and the distance from the sample to the tip. In α-(BEDT-TTF)$_2$I$_3$, BEDT-TTF donors locate in the same height on the $a-b$ surface unlike the case of θ-(BEDT-TTF)$_2$RbZn(SCN)$_4$ [40]. Therefore, the difference in the tunneling current originates from that in the electronic density of states. X-ray diffraction [18] and ^{13}C-NMR [17, 41] measurements reported that the charge on B molecule is richer than that on C molecule above $T_{\rm CO}$. Taking into account these results, we assigned B(C) molecules as brighter (darker) spots along the columns indicated by arrows, and the column indicated by arrows is the column II and another is the col-

umn I. The spots at diagonally upper (lower) side of B molecule are assigned as A(A') temporarily for the discussion.

In order to discuss the charge disproportionation in detail, we took line profiles along columns I and II. The profiles are averaged over width of a column (0.46 nm) to evaluate the charge distribution in each columns. Figure 3.2 shows line profiles. Red and blue lines represent column I and II, respectively. The two-fold periodicity was clearly observed in the line profiles of Columns II, a, c and e. The two-fold periodicity with charge rich A molecules was also observed in the profiles on the column I. The charge disproportionation along column I and II are consistent with the previous work [42]. The two-fold periodicities in both columns I and II form stripe structure with horizontal type, which is similar to the structure in charge ordered state, at room temperature. Moreover, in this study, we found that the stripe structure is formed with some inhomogeneity by observing the charge distribution on the BEDT-TTF layer in detail. The amplitude of the modulation in the columns I is weaker than that in the columns II. The ratio of charge amount of charge rich and poor molecules depends on the position in contrast to the two-fold periodicity on columns II. In the region indicated by the rectangle, uniform charge distribution domain was observed.

There might be a possibility that the observed stripe structure originates from some surface reconstruction. In organic conductors, the intra-molecular surface reconstruction is expected to occur as well as inter-molecular surface reconstruction, since the donor and anion molecules also consist of many atoms. Ethylene groups of a BEDT-TTF molecule in bulk are distorted due to the electrostatic interaction with anion layer. On the other hand, the ethylene groups closest to surface are not distorted, since they are free from anion molecules. Such surface reconstructions have been reported by STM in organic conductor β-(BEDT-TTF)$_2$PF$_6$ [43]. The inter-molecular case was observed as the arrangement alternating bright and less bright columns. The surface reconstruction can be explained by the mechanism similar to Si(100) and GaAs(100). On the outer columns, it was observed, a large spot which corresponds to a BEDT-TTF molecule with the relaxed ethylene group closest to the surface. On the inner columns two spots with different size and brightness was observed as a non-relaxed BEDT-TTF molecule. One is a large and bright spot, and another is a small and less bright spot. In the present STM results, only

relaxed BEDT-TTF molecules were observed . If the horizontal stripe is the pattern of height variation due to inter-molecular surface reconstruction, the spots of non-relaxed BEDT-TTF molecules must be also observed at less bright peak of two fold modulation. However, there is no non-relaxed BEDT-TTF molecules in the STM image. Therefore, the possibility that horizontal stripe is due to the surface reconstruction can be excluded.

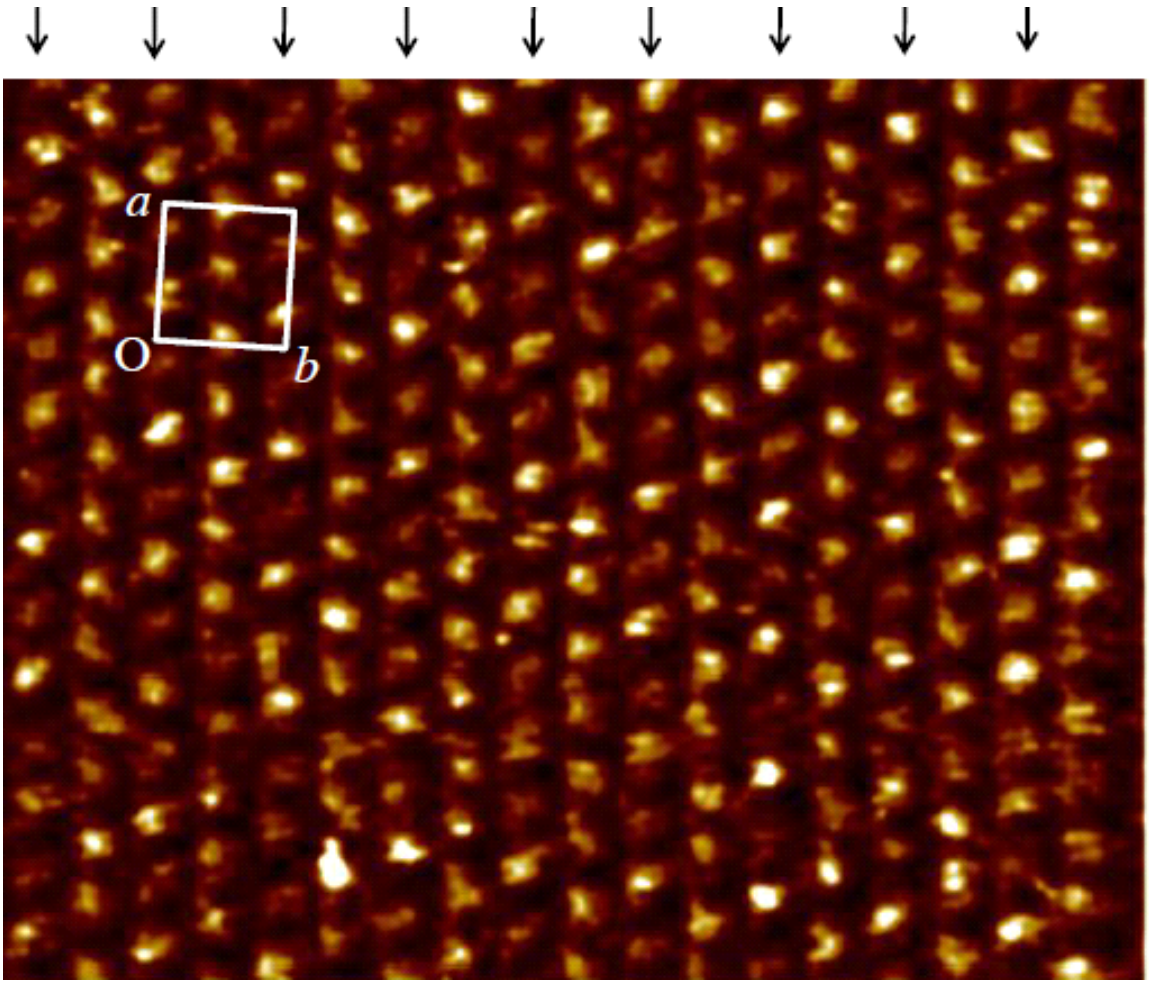

Figure 3.1: Current image on the $a-b$ plane at the bias voltage $V = 50$ mV and the tunneling current $I = 50$ pA. A white rectangle indicates the unit cell of the BEDT-TTF molecule arrangement in the image. The scanning area is 9.4×6.2 nm^2.

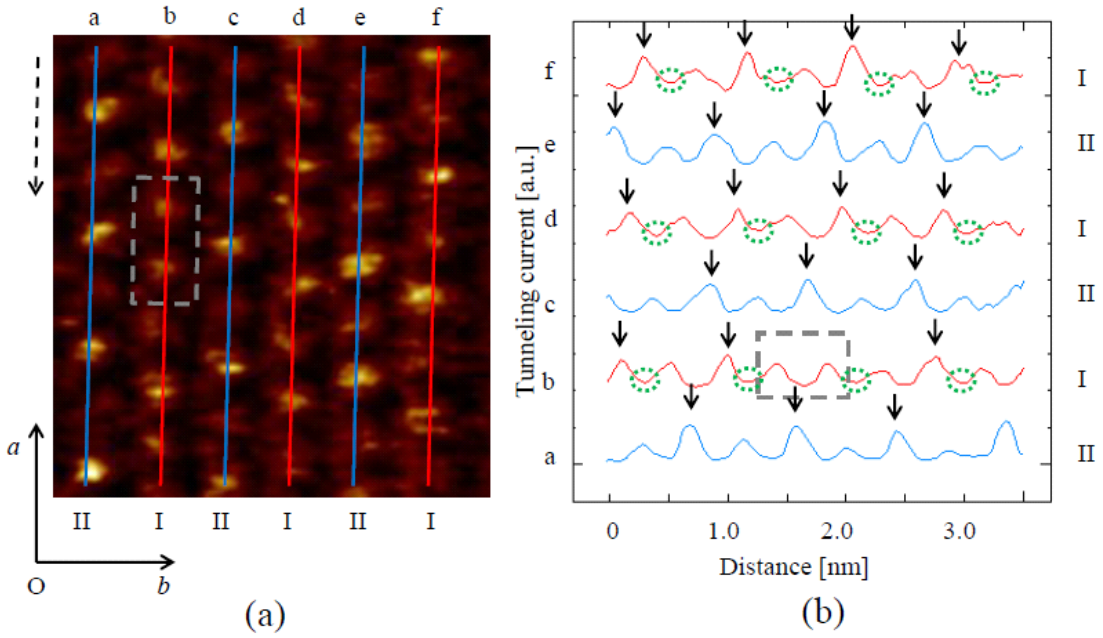

Figure 3.2: (a) An STM image with the same bias voltage and tunneling current as Fig. 3.13.1. (b) Line profiles along the columns. An arrow at the left side of (a) represents the direction, along which profiles were taken. Arrows in (b) indicate charge rich molecules. Gray rectangles in (a) and (b) indicate the charge uniform part.

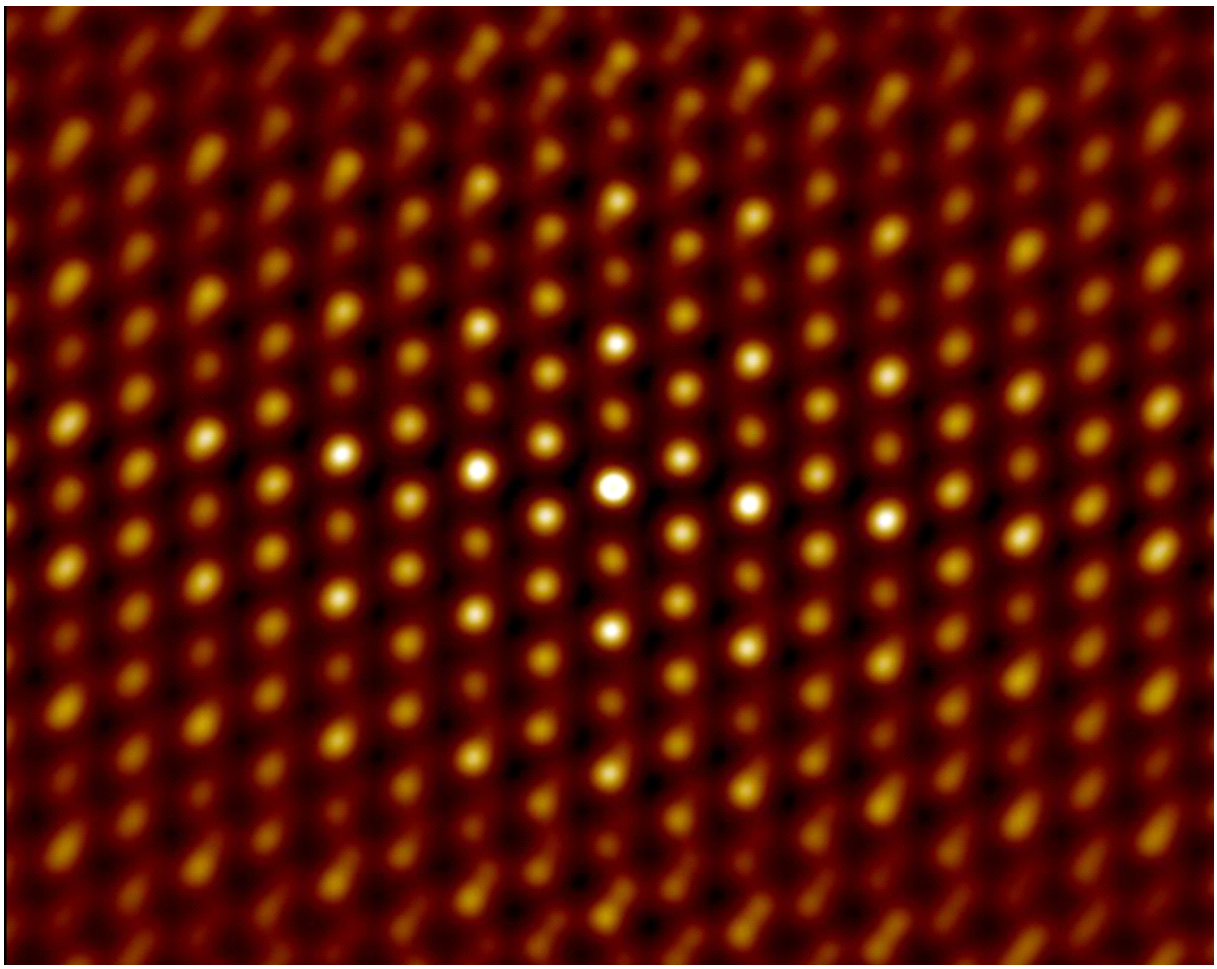

Figure 3.3: Autocorrelation image of Fig. 3.1.

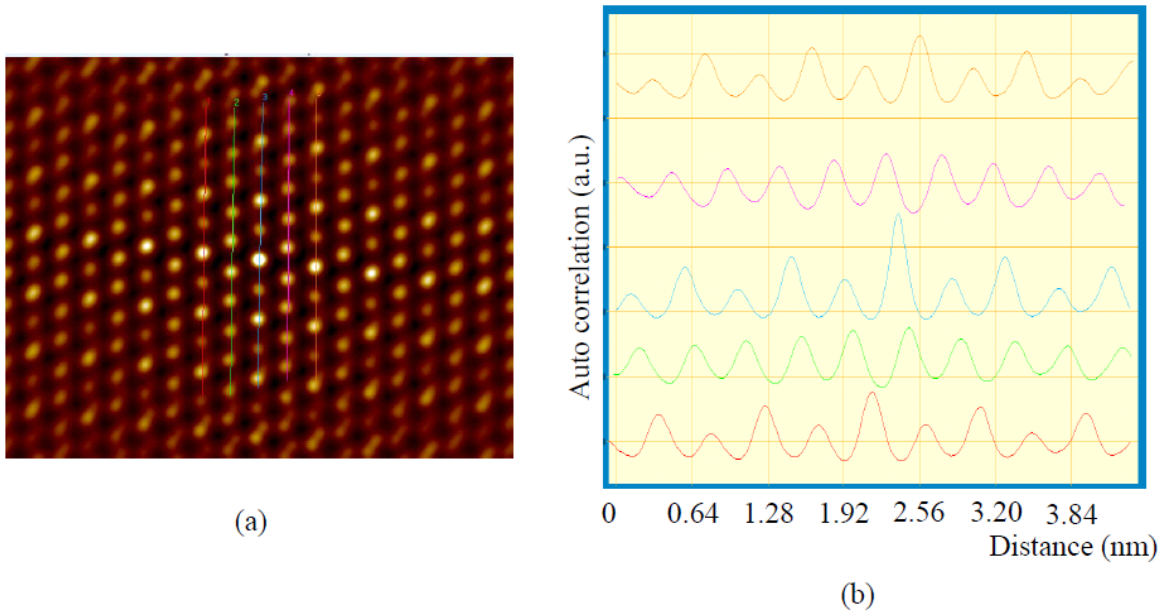

(a)

(b)

Figure 3.4: (b) Line profiles of Fig. 3.3 along columns. Numbers of profiles in (b) correspond to those of lines in (a).

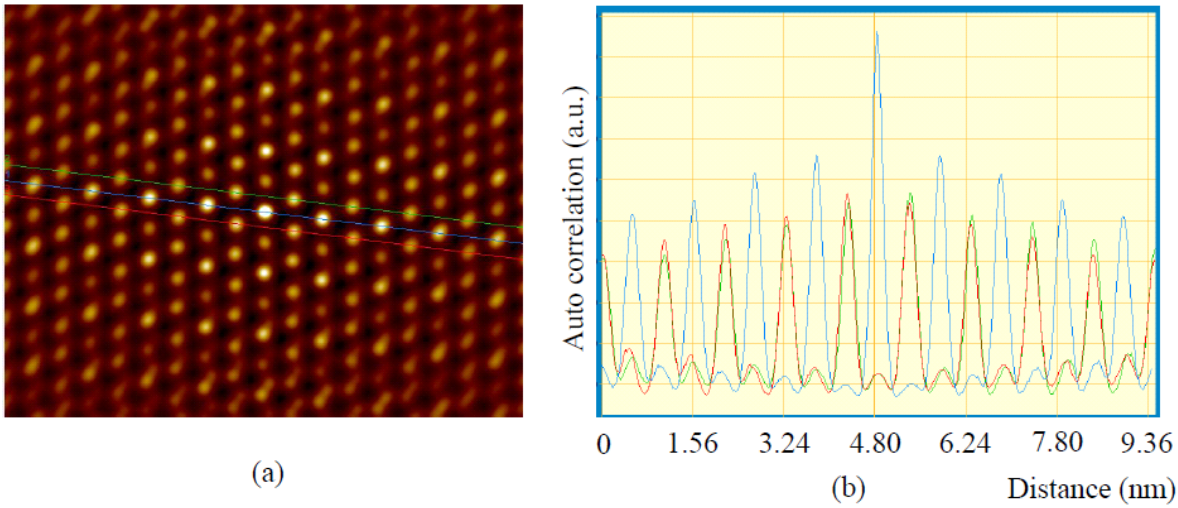

Figure 3.5: (b) Line profiles of Fig. 3.3 along inter-columns direction. Numbers of profiles in (b) correspond to those of lines in (a).

3.1.2 Charge stripe with charge rich A molecules

The stripe structure in the figure, in which molecules A' are charge rich, was also observed in different area. Figure 3.6 shows the line profiles in the area, where the stripe structure with charge rich A' molecules was observed. The two-fold periodicity develops in the whole area of Fig. 3.6 (a). I noticed that the phase of the charge modulation in profile "j" is an inversion of that in profile "h". The charge modulation in profile "h" is the two-fold periodicity with charge rich A molecules, which is the same as that in Fig. 3.2, while A' site is rich in profile "j". The two-fold periodicity with charge rich A' molecules forms the stripe structure. The horizontal stripe structure with charge rich A' molecules was formed in columns, i, j and k. In the area surrounded by green line in Fig. 3.6 (a), which corresponds to the boundary between A rich and A' rich horizontal stripe, A(column h), B(column i) and A'(column j) molecules are charge rich sites. They form diagonal stripe (Fig. 1.6 (c)).

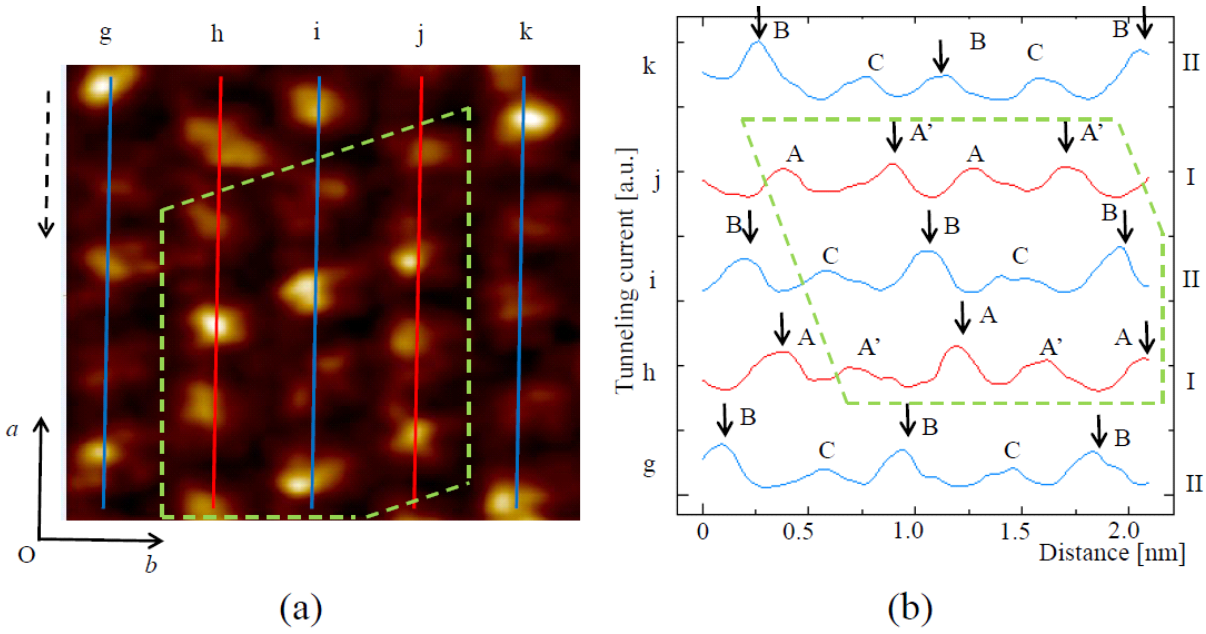

Figure 3.6: (a) STM image around the column I developing two-fold periodicity with charge rich A' molecules. (b) Line profiles in (a). An arrow with the broken line represents the direction of the horizontal axis of (b). Arrows in (b) indicate the charge rich molecules.

3.1.3 Domain structures

The charge distribution was mapped to evaluate stripe pattern. We reexamine the current image (Fig. 3.1) in Fig. 3.7 (a) and (b). Figure 3.7 (a) shows STM current image. We mapped donor sites in Fig. 3.7 (b) classifying three types, which are charge rich, poor and non-classified sites. Red, blue and white ellipses represent charge rich, poor and non-classified sites, respectively. In some parts of column I, the charge is regarded as uniform as indicated by white rectangle with broken lines in Fig. 3.7 (a) and white ellipses in Fig. 3.7 (b). It corresponds to non-classified site. The two fold periodicity along column II with charge rich B molecules develops in whole observed area. I note again that the alternation in column II is strict, *i.e.* site B is charge rich and C is poor. The horizontal stripe structure with charge rich A molecules develops in most of the observed area. In column I, modulation of the two-fold periodicity is weaker than that in column II as described above. The ratio of the electron density on the charge rich and poor molecules varies depending on the position in contrast to that in column II as shown in Figs. 3.2 and 3.6. In the parts of column I denoted by white ellipses in Fig. 3.7 (b), the alternation between charge rich and poor is not clear. Then it seems that although A site rich horizontal stripe order develops almost whole observed area, the coherence is divided by non-classified sites, in which no charge disproportionation occurs. Additionally, in green rectangle in Fig.3.7 (a) and (b), diagonal stripes are formed locally. Both cases of A rich and A' rich horizontal stripes are degenerated since A and A' molecules are crystallographically equivalent. It might be possible that A' rich horizontal stripe develops in other area. On the boundary between A rich and A' rich horizontal stripes, diagonal stripes are formed. Such domains have been observed as domains with opposite polarization even in charge ordered state by the optical measurement with second-harmonic generation [44]. Even in the charge ordered state, it is expected that diagonal stripe exists as a domain wall between domains of the horizontal stripe structures with charge rich A and A'.

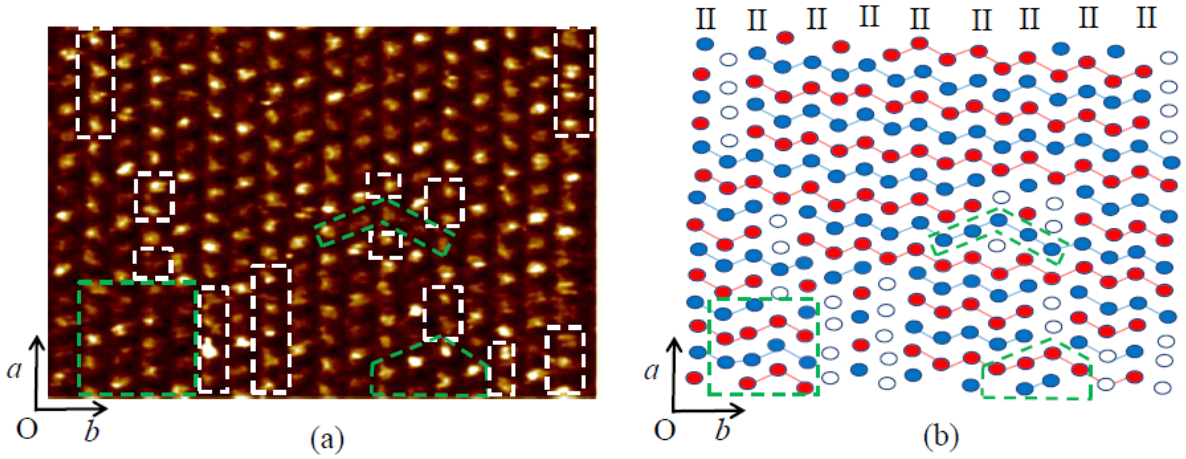

Figure 3.7: Mapping of BEDT-TTF donor sites. (a) STM current image (as the same as Fig. 3.1). (b) Schema of donor sites. Red, blue and white ellipses represent the charge rich, poor and non-classified sites, respectively.

3.2 α-(BEDT-TTF)$_2$KHg(SCN)$_4$

Figure 3.8 shows an STM image of α-(BEDT-TTF)$_2$KHg(SCN)$_4$ with the tunneling current of 0.5 nA at bias voltage of 15 mV. The scanning area is 4.4 $\times$ 3.7 nm^2. α-tyepe donor arrangement was clearly observed as in the case of α-(BEDT-TTF)$_2$I$_3$. The dimension of the unit cell indicated by a white square is 1.03 $\times$ 1.03 nm^2, which is consistent with the lattice parameter. The STM image was identified as the image on the donor layer of α-(BEDT-TTF)$_2$KHg(SCN)$_4$. In the image, it was also observed that the tunneling current varies depending on the donor sites. However, the two-fold charge modulation on a large area was not observed in contrast to the case of α-(BEDT-TTF)$_2$I$_3$. Therefore, the spots in the image could not be assigned with A, A', B and C.

In order to discuss the charge distribution on the donor layer of K salt, line profiles were taken along each columns. Figure 3.9 shows the line profiles. The horizontal charge stripe similarly to the case of I$_3$ salt was found in K salts. The two-fold charge modulation was observed along each column. The modulation with some inhomogeneity forms the horizontal charge stripes. The wave vector of the charge modulation is similar to that of the charge order in I$_3$ salts rather than that of the density waves in K salts [45]. However, the charge modulation along whole column was not observed even in the profiles. It was

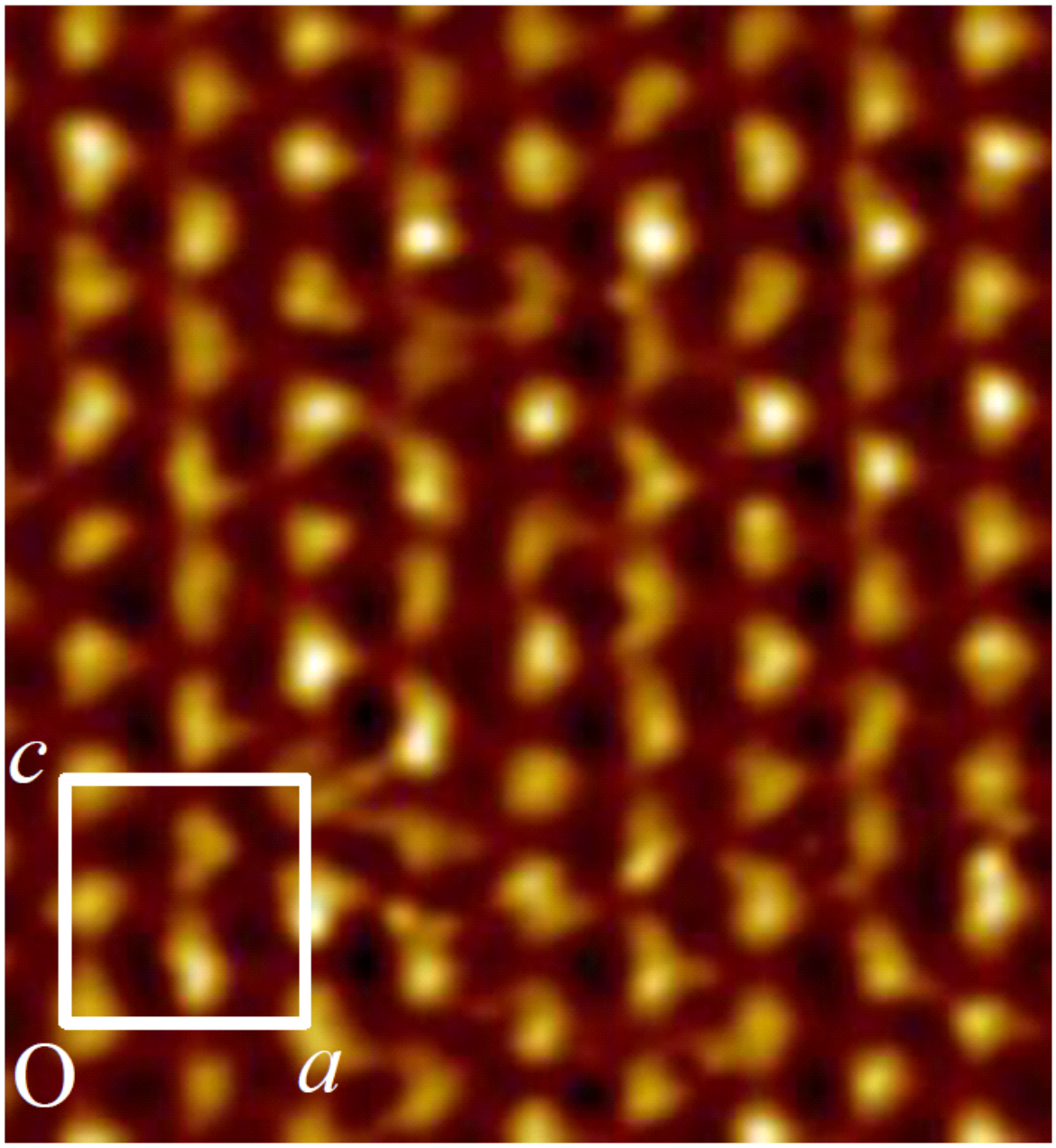

Figure 3.8: STM current image of α-(BEDT-TTF)$_2$RbHg(SCN)$_4$ at tunneling current I = 0.5 nA and bias voltage V = 15 mV with scanning area of 4.4 nm $\times$ 3.7 nm

confirmed to essentially exist by the image mapped auto-correlation function on as shown Fig. 3.10, 3.11 and 3.12. The correlation length of the modulation is shorter than that of I_3 salt, and the amplitude is also smaller than that of I_3 salt. The charge stripe structure is found to be more unstable than that of I_3 salts.

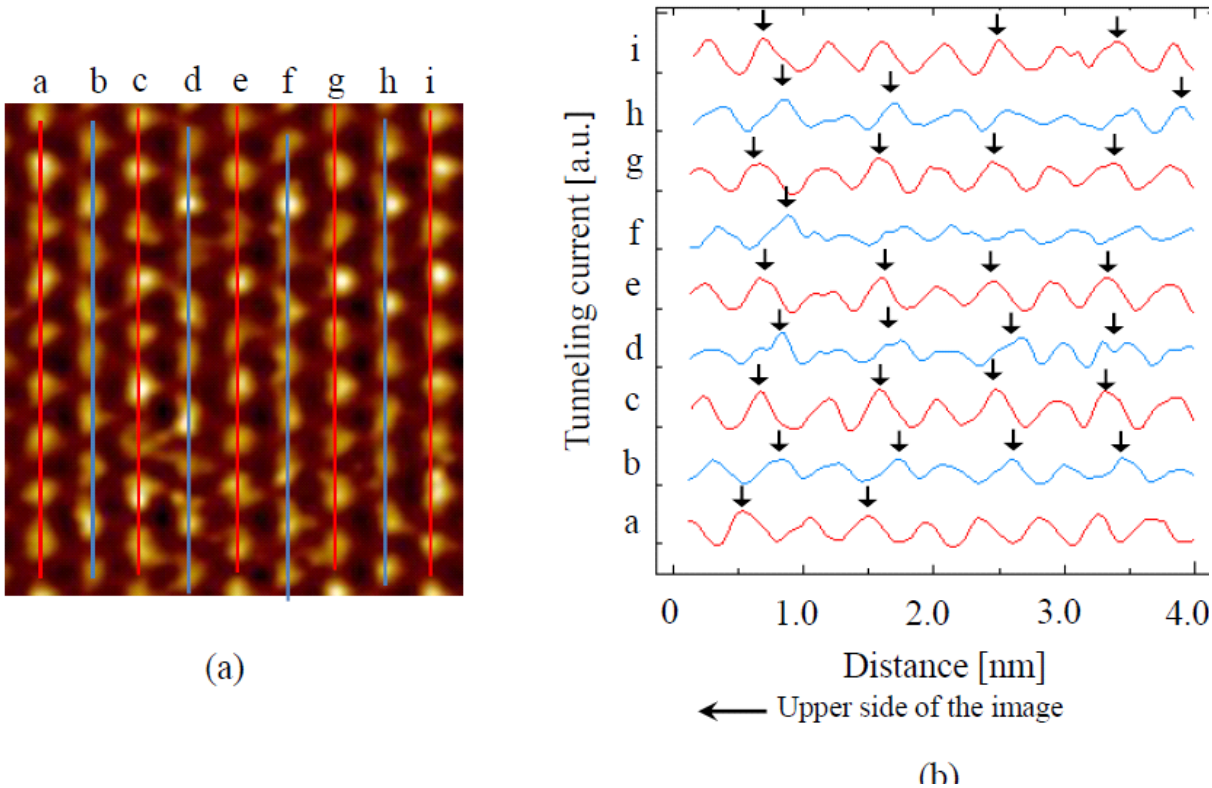

Figure 3.9: (b) Line profiles along columns of Fig.3.8. Arrows in (b) indicate molecules with charge rich. Alphabets of profiles in (b) correspond to those of lines in (a).

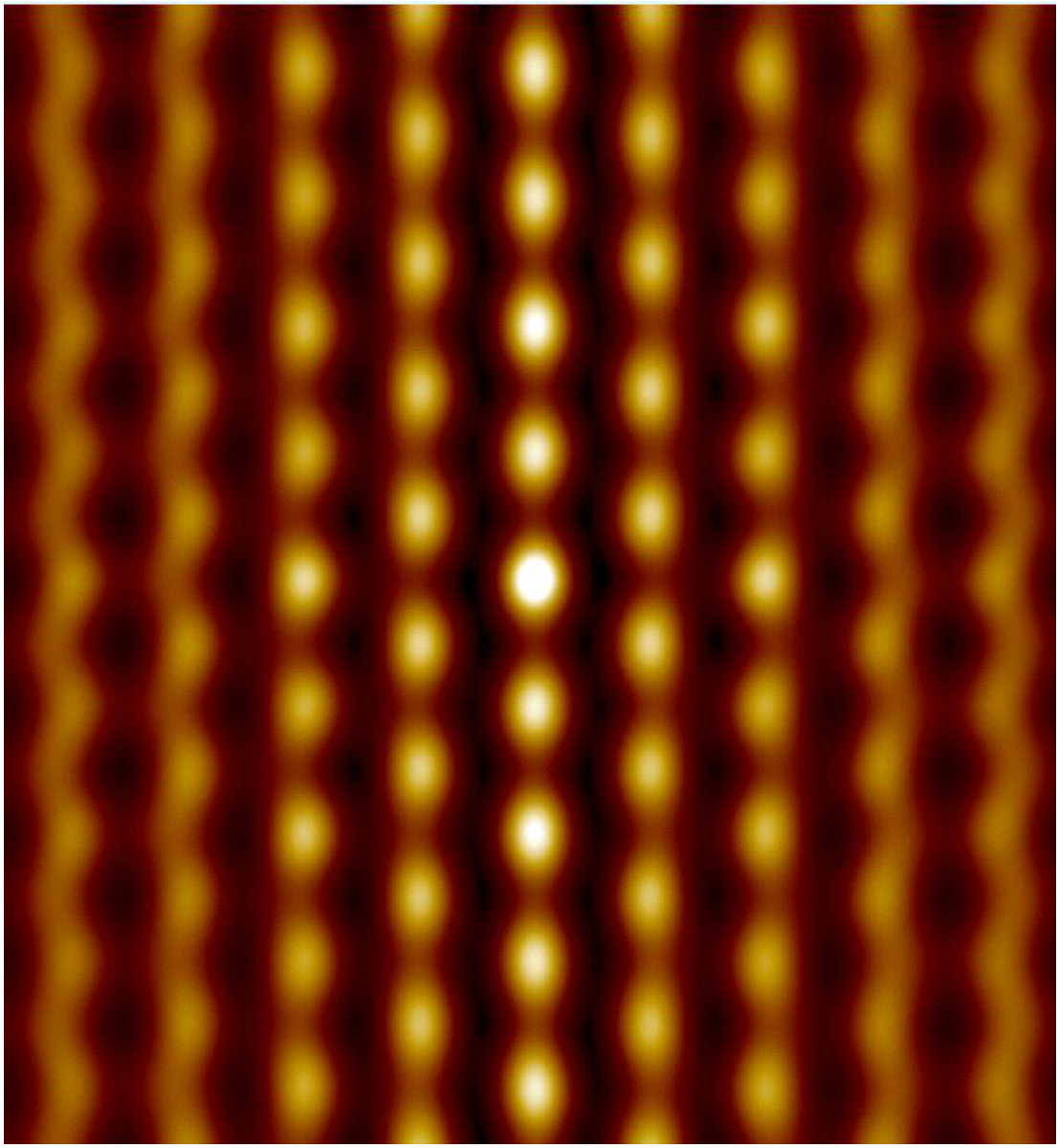

Figure 3.10: Autocorrelation image of Fig. 3.10.

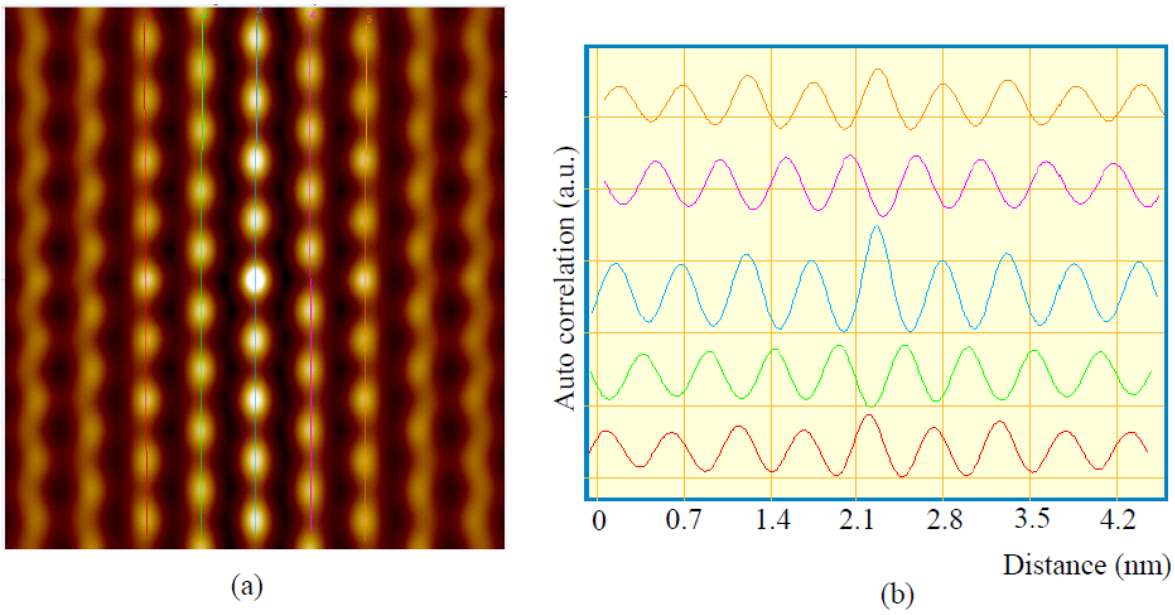

Figure 3.11: (b) Line profiles of Fig. 3.10 along columns. Numbers of profiles in (b) correspond to those of lines in (a).

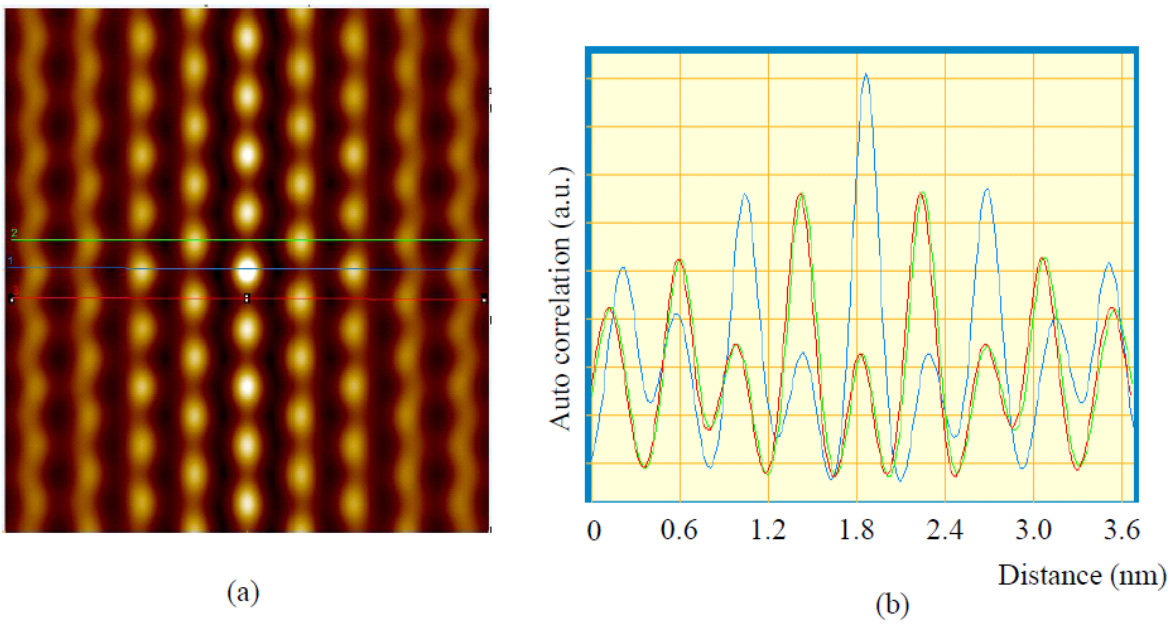

Figure 3.12: (b) Line profiles of Fig. 3.10 along inter-columns direction. Numbers of profiles in (b) correspond to those of lines in (a).

3.3 α-(BEDT-TTF)$_2$RbHg(SCN)$_4$

The vertical charge stripe structure (Fig. 1.6) was observed in Rb salt. Figure 3.13 shows the current image of Rb salt. α-type donor arrangement with the dimension of the unit, 1.03×1.05 nm^2, was clearly observed. The dimension is consistent with the lattice parameter of Rb salt, $a = 1.0061$ nm and $b = 0.9976$ nm. Mover, vertical charge stripe, in which charge aligned along columns, was clearly observed without any inhomogeneity in Rb salt. The result with vertical charge stripe is consistent with the ^{13}C-NMR result [46], in which the vertical charge stripe was also reported from knight shifts of each crystallographically non-equivalent donor sites. The vertical stripe structure is completely different from the horizontal stripe observed in K salt.

In order to discuss about the charge modulation in the direction along and perpendicular to the columns, line profiles were taken along a few directions. Figure 3.14 (b) shows the line profile in the direction along and across the columns. The profiles "a" to "d" are along columns, and the profiles "e" and "f" are in the direction across columns. The origin of the profiles "e" and "f" correspond to the right end of the lines in Fig. 3.14 (a).

The two-fold charge modulation was also observed on the profiles along columns locally. Parts of the column developing the charge modulation were placed apart. In other words, the two-fold charge modulation along columns do not form horizontal stripe structure. On the other hand, the two fold modulation along the inter-column direction was clearly observed in the whole area observed by STM. The dimerizations of molecules in Column I and II was also observed as the alternate alignment of the shallow and deep dips similarly to the dips along column I for I_3 salt. They were confirmed to essentially exist by the image mapped autocorrelation function on as shown Fig. 3.15 ,3.16 and 3.17.

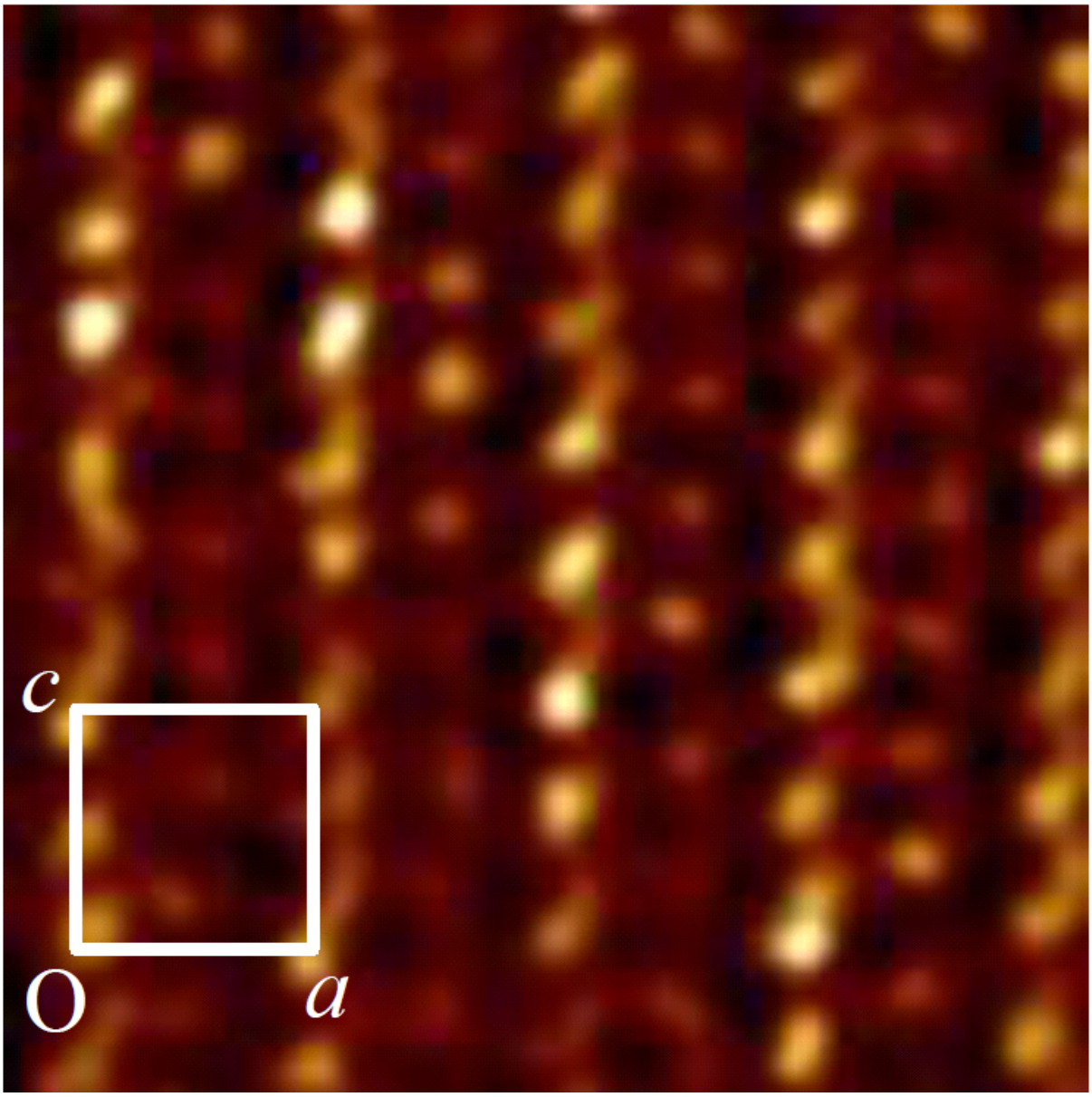

Figure 3.13: STM current image of α-(BEDT-TTF)$_2$RbHg(SCN)$_4$ at tunneling current I = 0.1 nA and bias voltage V = 15 mV with scanning area of 4.3 nm $\times$ 4.2 nm.

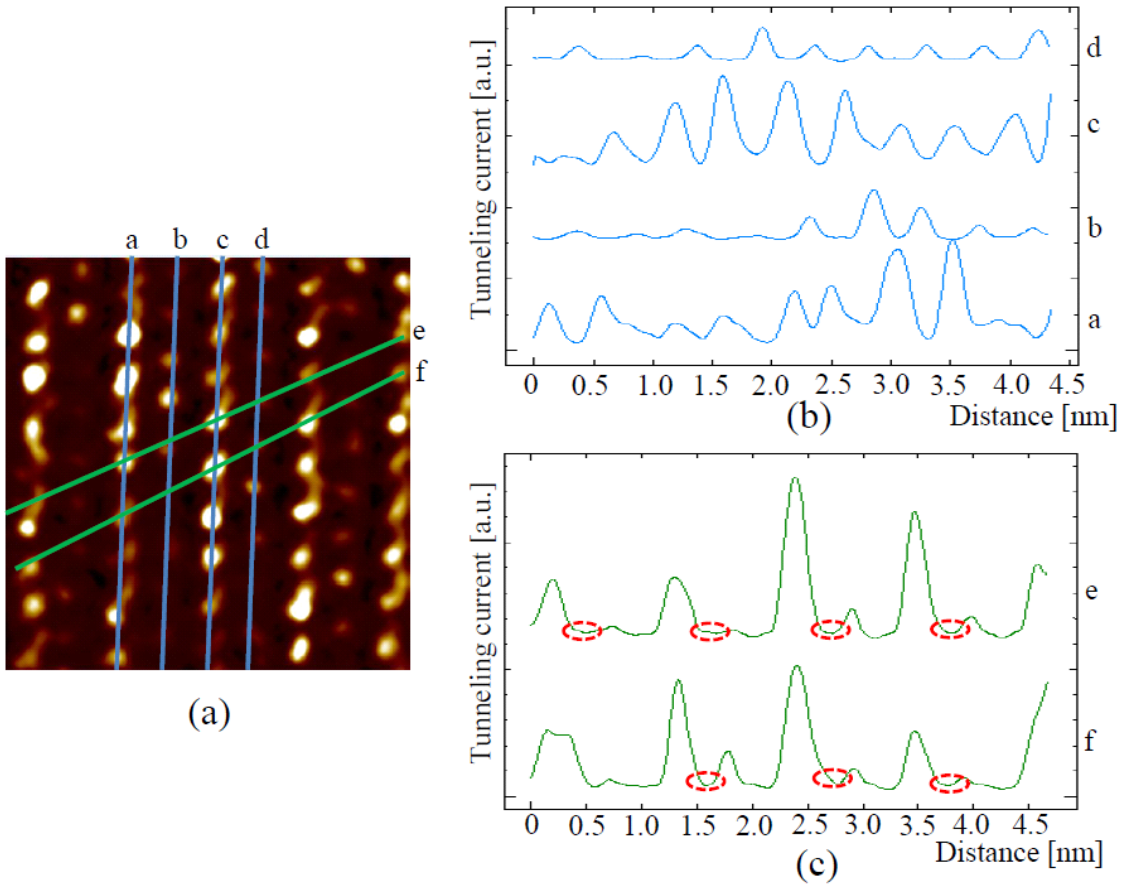

Figure 3.14: Line profiles along (b) columns and (c) inter-columns direction of 3.13. Red circles with break lines in (c) indicate shallow dips. Alphabets of profiles in (b) correspond to those of lines in (a).

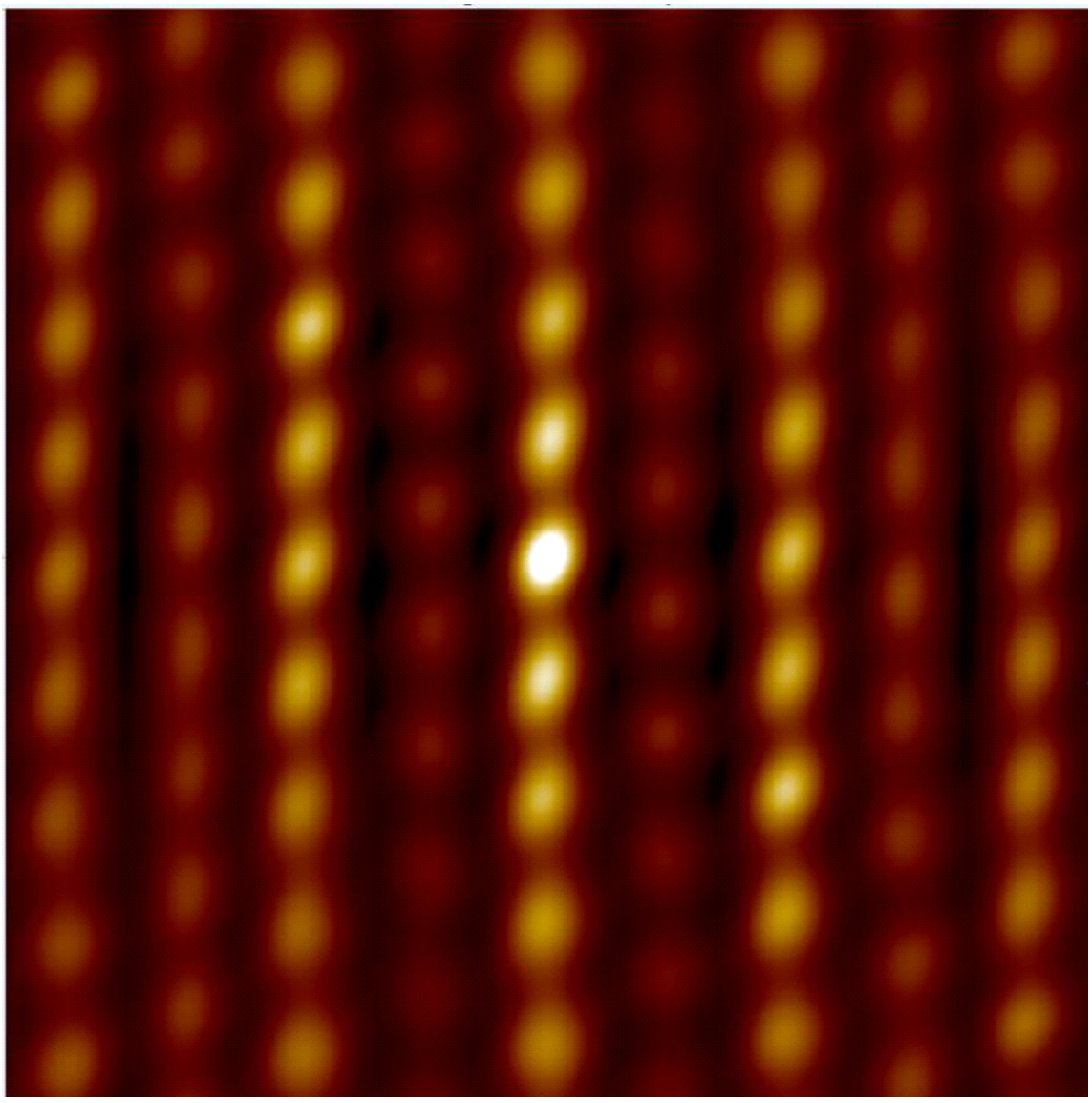

Figure 3.15: Autocorrelation image of Fig. 3.13.

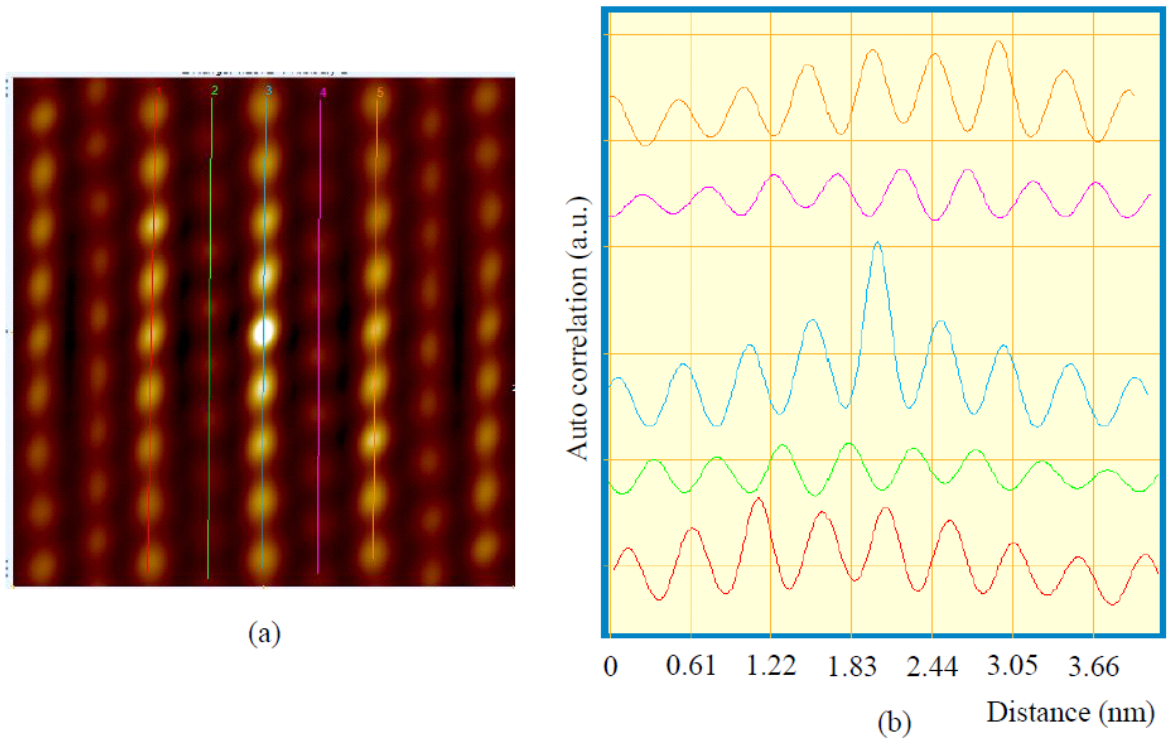

Figure 3.16: (b) Line profiles of Fig. 3.15 along columns. Numbers of profiles in (b) correspond to those of lines in (a).

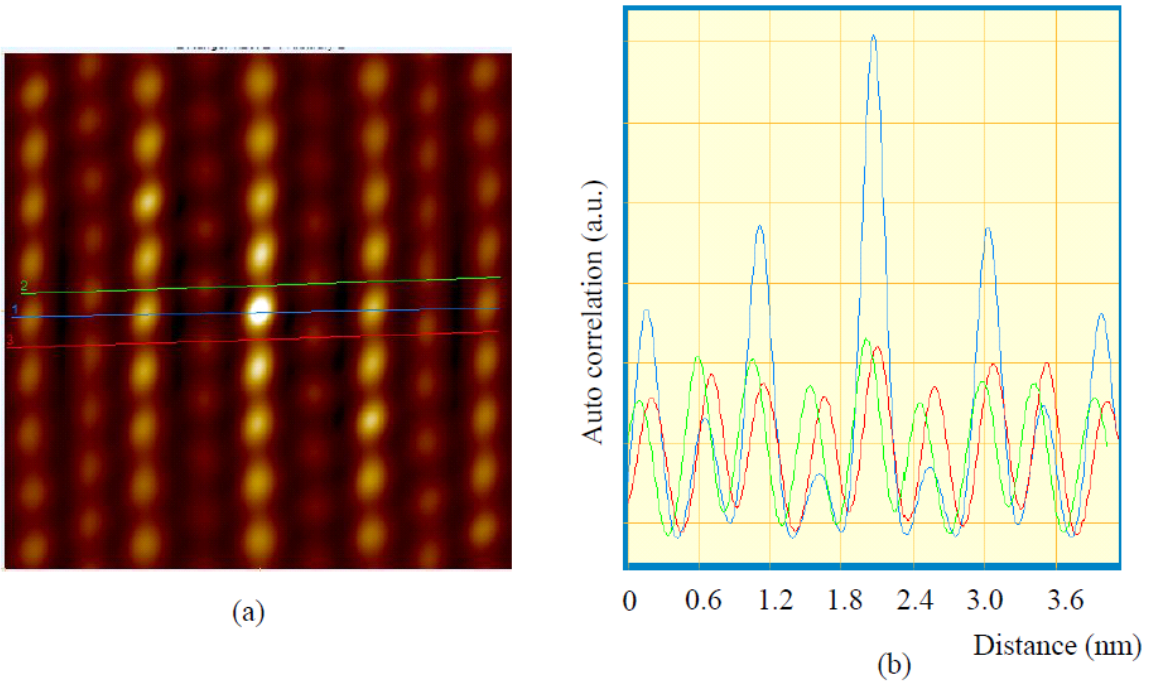

Figure 3.17: (b) Line profiles of Fig. 3.15 along inter-columns direction. Numbers of profiles in (b) correspond to those of lines in (a).

Chapter 4

Discussion

4.1 Effect of anion layer on the charge distribution

I will discuss about the amplitude of the charge modulation along Column II of I_3 salt in this section. I note that the charge modulation along Column II of I_3 salt has larger amplitude than that of K and Rb salts observed by the present STM study, and exists stably in the whole area observed by STM. I focus on the anion arrangement of I_3. Figure 4.1 and 4.2 show BEDT-TTF and anion molecule arrangement in I_3 and K salt, respectively. These are the view from the direction stacking BEDT-TTF layers and anion layers alternately. To estimate the effect of anion layers, only SCN molecules closest to a BEDT-TTF layer and the outer ring of BEDT-TTF closest to an anion layer are shown in the figure. The arrangement for Rb salt can be understood by replacing potassium atoms in Fig. 4.2 with rubidium atoms.

Hydrogen atoms of BEDT-TTF molecules lie near an anion layer. Hydrogen atoms are expected to be affected by the negative electrostatic potential of an anion layer. In I_3 salt, first principle density function theory (DFT) calculation reported that negative charge concentrates on terminal iodines of I_3 molecules [47]. In K (Rb) salt, sulfur and nitrogen atoms of SCN lie near Hg^{2+} and K^+ (Rb^+) in an anion layer, and these are closest to hydrogens of BEDT-TTF. Since electronegativity of nitrogen is larger than that of sulfur although sulfur lies near Hg^{2+}, it is expected that negative charge on the anion layer concentrates on the terminal atoms of SCN, sulfur and nitrogen, with same amount of charge. Taking into account the negative charge distribution in anion layers,

lengths of hydrogen bonds are indicated by green characters. The length of hydrogen bond increases in order corresponding to B site, A (A') site, C site in I_3 salt. In K salt, the length of hydrogen bonds of A and A' sites on Column I are shorter than those of B and C sites on Column II. The arrangements of hydrogen bonds in I_3 salt and K salt are similar to the charge distribution on I_3 and Rb salt. As mentioned above, Rb salt has the same arrangement of hydrogen bonds as K salt, since Rb salt has almost the same crystal structure as K salt. It is expected that the charge distribution on a BEDT-TTF layer is expected to be modified by hydrogen bonds between ethylene groups and anions.

Although, it is unnatural that hydrogen bonds interact directly with charge of π-orbital which forms conduction band, since it does not exist around the ethylene group of a BEDT-TTF molecule in bulk. On other hand, the charge on a σ bond of BEDT-TTF exists around the ethylene groups of a BEDT-TTF molecule. The positive charge is attracted by the negative charge of a ion forming hydrogen bonds with a BEDT-TTF molecule. Charge of the π-orbital existing around the center of a BEDT-TTF molecule feels the potential by the concentration of positive charge of σ orbital. Therefore, the large charge modulation on Column II of I_3 salt and the homogeneous vertical stripe on Rb salt is expected to be stabilized by the potential originates from hydrogen bonds.

However, the charge distribution on K salt is similar to that of I_3, in which the horizontal stripe was observed in contrast to Rb salt, despite of the fact that the negative electrostatic potential due to the arrangement of hydrogen bonds favors the vertical stripe rather than the horizontal stripe in the K and Rb salts. This suggests that there is another factor determining the charge structure which leads charge distribution of K salt to the horizontal charge stripe. If the horizontal stripe coexists with the vertical stripe, the energy of donor layer increases by the amount of on-site Coulomb energy since a double occupied site exists in the unit cell. The coexistent state is unstable, and the horizontal stripe on K salt is expected to be more unstable than that on I_3. Actually the horizontal stripe of K salt is more inhomogeneous than that of I_3 salt.

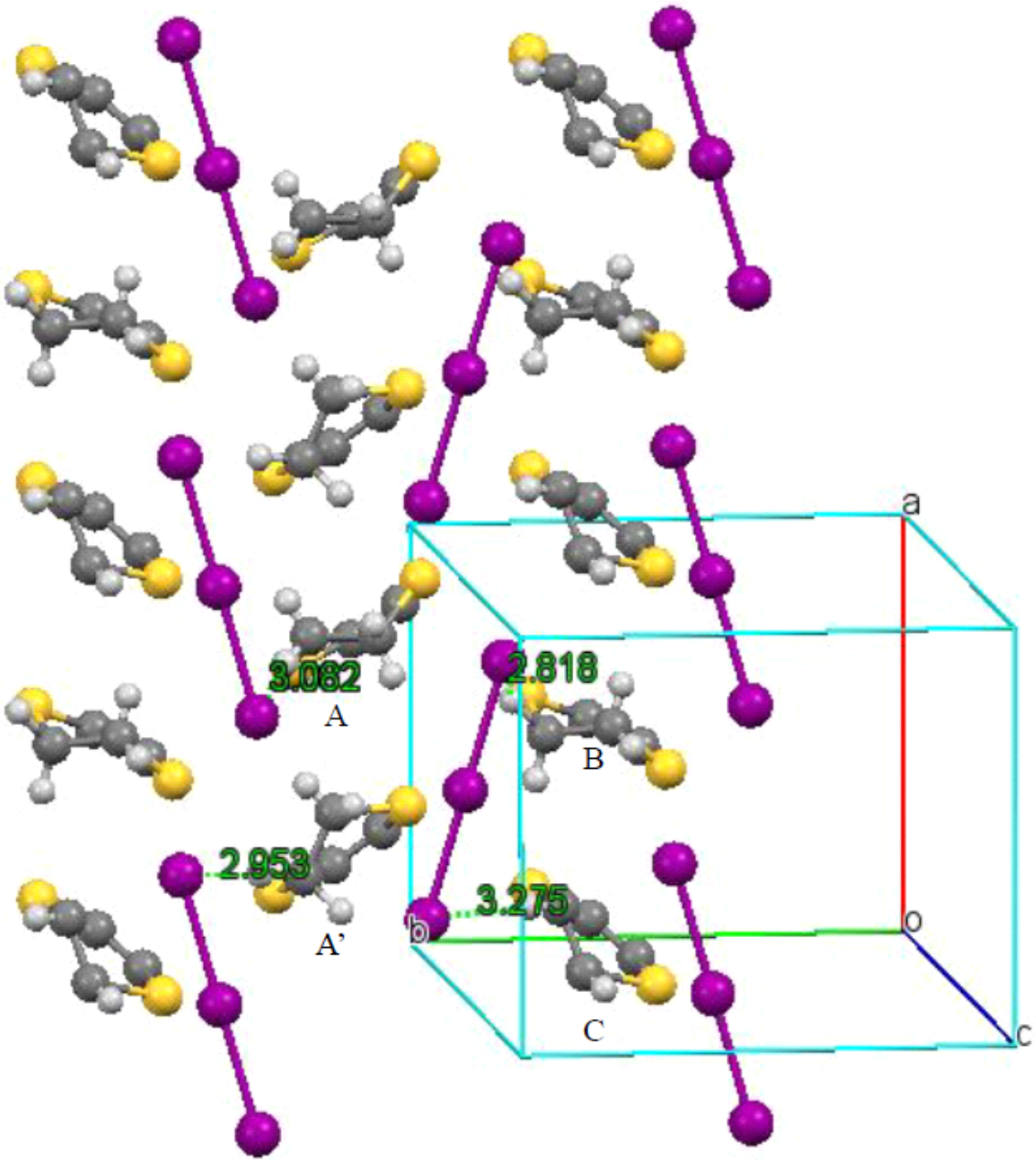

Figure 4.1: Crystal structure of α-(BEDT-TTF)$_2$I$_3$ along the c^* direction. Green numbers in the figure are hydrogen bond lengths between the hydrogen of a BEDT-TTF closest to I_3^- and end of the I_3^-.

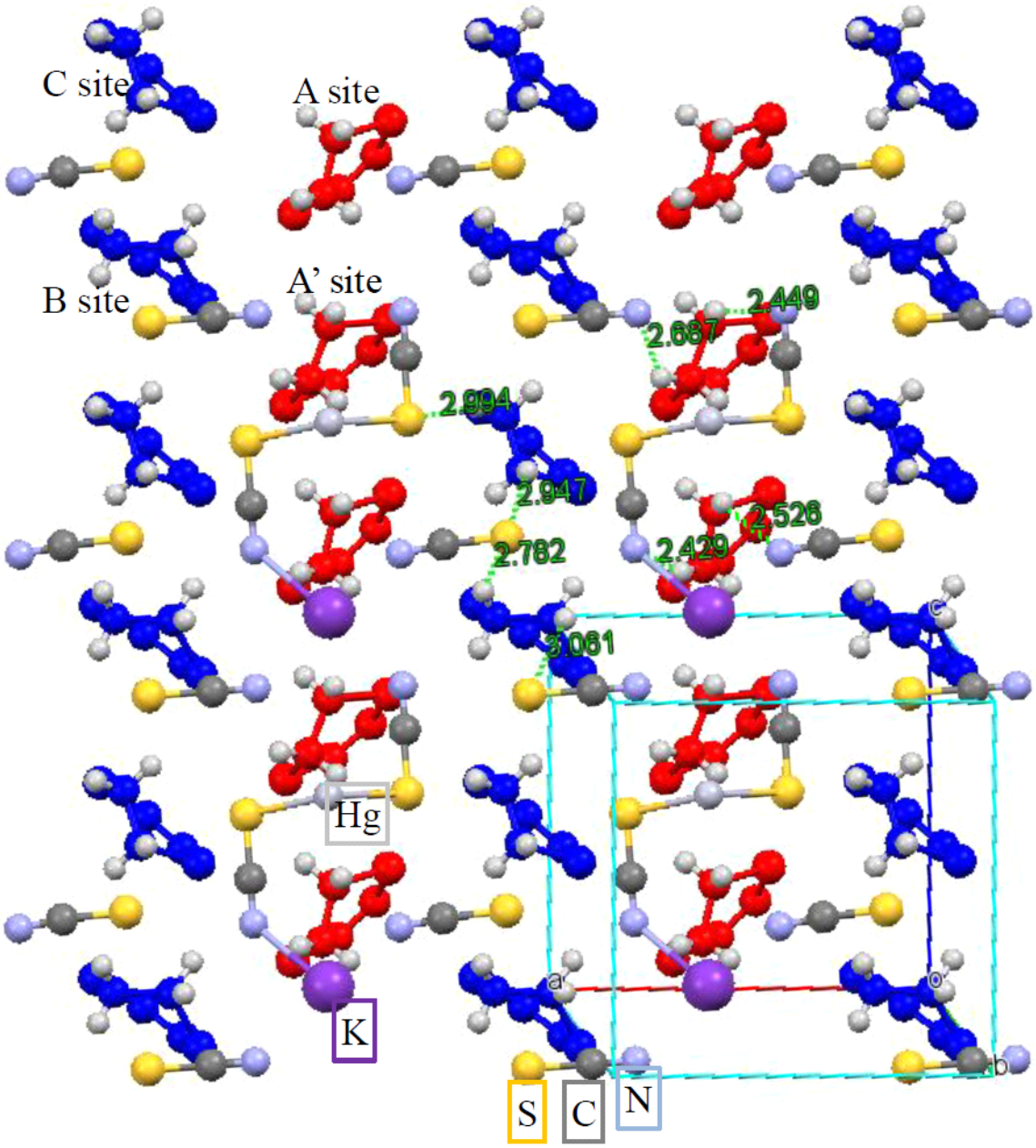

Figure 4.2: Crystal structure of α-(BEDT-TTF)$_2$KHg(SCN)$_4$ along the b^* direction. Green numbers in the figure are hydrogen bond lengths between the hydrogen of a BEDT-TTF closest to SCN^- and a sulfur or a nitrogen of the SCN^-. We focus on a sulfur and a nitrogen of SCN^- in an anion layer, since they are located near a mercury ion with positive divalent and a potassium ion with positive monovalent and SCN^-s are more closer to BEDT-TTF layer. BEDT-TTFs with red and blue belong to Column I and Column II, respectively.

4.2 Effect of dimerization on the charge stripe

First I will discuss about the dip arrangement on STM images. I note dips along column I in I_3salt. Shallow dips along the column I are indicated by green circles in Fig. 3.2 (b). Shallow and deep dips are aligned alternately along column I. It indicates the dimerization between A and A'. On the other hand, such an alternation of dips was not observed along the column II. I emphasize that the dimerization observed by STM reflects the electronic state. The electron density between BEDT-TTF molecules corresponds to the transfer integral. In α-type donor arrangement above $T_{\rm CO}$, while molecules A and A' are weakly dimerized, molecules B and C are not. Below $T_{\rm CO}$, X-ray diffraction suggested that a rearrangement of donor molecules and it results in the dimerization even between B and C, whose transfer integral is almost equal to that of A-A' dimer [33, 18]. Present STM observation about the donor arrangement is consistent with crystallographical results [33] above $T_{\rm CO}$ and indicates no donor re-arrangement in contrast to that below $T_{\rm CO}$. I conclude that the charge disproportionation state develops on the donor arrangement which differs from that at the charge ordered state below $T_{\rm CO}$. I notice that the horizontal stripe observed at room temperature is accompanied by some inhomogeneity. From the permittivity measurement in θ-(BEDT-TTF)$_2$RbZn(SCN)$_4$ [22], $T_{\rm CO}$ decreases with increasing the cooling rate, which affects to suppress the coherence of the structural change such as the dimerization between B and C. Moreover, X-ray diffraction suggested that the diffuse of $\boldsymbol{q} = (1/3\ k\ 1/4)$ corresponding to charge disproportionation still remains below $T_{\rm CO}$ for the fast cooling rate (9 - 10 K/min) in contrast to the case of slow cooling (0.1-0.2 K/min) [48]. It might be understood that the dimerization between B and C stabilizes the charge stripe with the long range order below $T_{\rm CO}$. Some inhomogeneity of the charge stripe is expected to be caused by the absent of dimerization between the dimer between B and C. Besides, I also found the dimerization perpendicular to the direction, in which charge of the vertical stripe aligns, in the STM image of Rb salt as shown in Fig 3.14. Shallow dips reflecting dimerization are indicated by red circles with broken lines. Although the direction of the dimerization in the vertical stripe is perpendicular to that in the horizontal stripe, it is the same as the relation between the directions of the dimerization and the charge line of stripe structures. There might be a possibility that ferroelectricity plays an

important role to stabilize a charge stripe in the formation of it, since the dimerization occurs as ferroelectricity emerges.

On the other hand, no dip alignment reflecting dimerization was observed in K salt. Since the charge stripe competes with the potential originates from hydrogen bonds, dimerization is not expected to form due to instability of the charge stripe.

4.3 Classification of stripe structures

Three salts with α-type donor arrangement were studied by STM at room temperature. First, I compare the stripe structure with the ground states for three salts as listed in Table 4.1. Three salts have the donor arrangement with α-type but differ in the band structure and ground state. One is the charge order and other two are the density wave. However, in all salts, we found the charge stripe structure in the metallic state and that the stripe pattern varies depending on material. The factor determining the charge structure on a BEDT-TTF layer is an open problem, although one of factors, which affects charge structure on a BEDT-TTF layer, is understood as the potential due to hydrogen bonds with an anion layer.

I notice that the stripe structure at room temperature on I_3 salt is similar to the charge structure of the charge order below 135 K on it. Taking into account the fact that CO state occurs due to the off-site Coulomb interaction, the charge stripe at room temperature is expected to originate from the off-site Coulomb interaction similarly to the case of CO, since the Coulomb interaction does not depend on temperature. The strength of the off-site Coulomb interaction is not expected to differ among salts since these have almost the same electron density on a BEDT-TTF layer.

Focusing on the anisotropy of the off-site Coulomb interaction originated from the donor arrangement of each salts, I analyzed stripe structures of α-type BEDT-TTF salts. First, two conditions were assumed. One is that the off-site Coulomb interaction is determined by the distance between nearest neighbor molecules for simplicity. There are two characteristic distances in α-type donor arrangement. Figure 4.3 (a) shows the distances on α-type donor arrangement. One is the distance between the nearest neighbor molecules of neighboring columns, another is that between nearest neighbor molecules in

Table 4.1: Relation of the stripe structures and ground states of each salts

Name of salts	Stripe Structures	Ground states
I_3 salt	Horizontal stripe (inhomogeneity)	Charge Order (Horizontal stripe)
K salt	Horizontal stripe (inhomogeneity)	Density wave
Rb salt	Vertical stripe	Density wave

its column. In this study, I define the former distance as "D_1" and latter one as "D_2". The other assumed condition is that the difference of the Coulomb interaction is negligibly small, which originetes from different pairs of molecules. D_1 and D_2 are estimated from the lattice parameters on the layers as follows; $D_1 = 1/2\sqrt{x^2 + D_2^2}$, $D_2 = y/2$, where x is the lattice parameter along inter-column direction, y is that along intra-column direction. From D_1 and D_2, the parameter of anisotropic long range Coulomb interactions is calculated as D_1/D_2 which means the ratio of Coulomb potential on D_1 to that on D_2.

Figure 4.3 (b) shows the calculated D_1/D_2, which characterizes the anisotropy of the off-site Coulomb potential, for three salts with α-type donor arrangement. I found experimentally the boundary between the horizontal and vertical charge stripes in α-type BEDT-TTF salts. It should be noted that Rb salt at room temperature with vertical stripe has the smallest value of D_1/D_2, and I_3 and K salts and Rb salt at 11 K have larger values than that for Rb salt at room temperature. These results suggest that the horizontal stripe structure is formed on the salt in which the off-site Coulomb interaction along the intra-column direction is stronger than the critical value, and in the case with weak off-site Coulomb interaction, the vertical stripe is formed. Besides, NMR measurement reported that vertical charge stripe changes to horizontal charge stripe below 100 K in Rb salt, which has larger D_1/D_2 than K at room temperature at 11 K [46]. Therefore, the present result suggests that stripe structures in α-type BEDT-TTF salts are classified by the anisotropy of the Coulomb potential D_1/D_2, and the boundary of the horizontal and vertical stripes is located between K and Rb salts at room temperature.

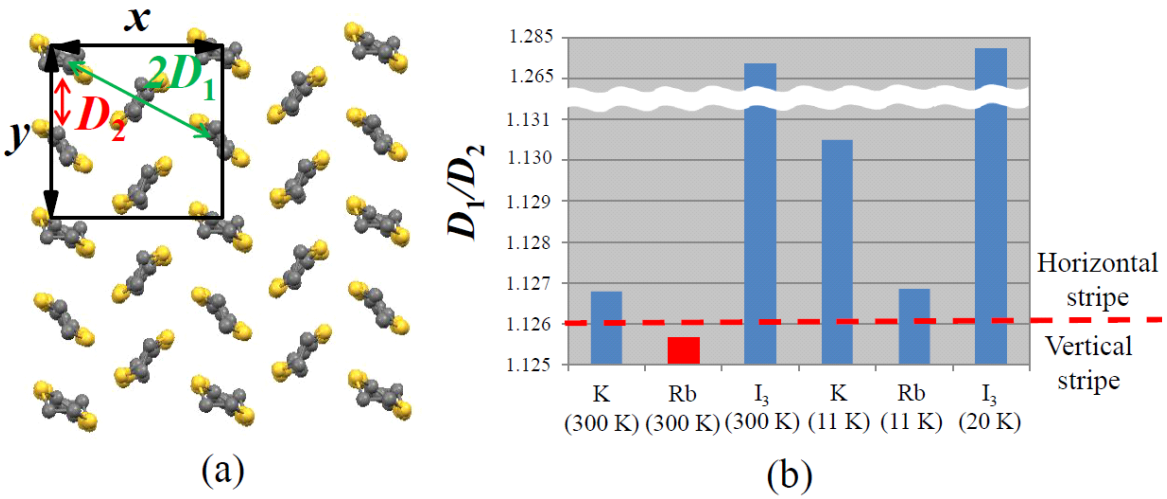

Figure 4.3: Schema about the definition of the parameter D_1/D_2, which means inhomogeneity of BEDT-TTF arrangement. D_1 is a distance between neighboring BEDT-TTFs along columns, and D_2 is one along inter-columns direction. x and y are dimensions of the unit cell along inter-columns and column directions. (b) Bar graph of D_1/D_2s for α-type BETDT-TTF compounds at room and low temperature. Blue bars are compounds with horizontal stripe citeNoda, and a red bar is one with vertical stripe.

Chapter 5

Conclusion

I performed STM observation on three α-type BEDT-TTF compounds, α-(BEDT-TTF)$_2$I$_3$ and α-(BEDT-TTF)$_2$MHg(SCN)$_4$ (M = K, Rb) to study the electron distribution at room temperature.. Single crystals of α-(BEDT-TTF)$_2$MHg (SCN)$_4$ (M = K, Rb) were successfully grown by the electro-chemical method. The density wave transition was clearly observed as a reduction of the static magnetic susceptibility in both M = K and Rb salts. Charge stripe structures were observed in the three compounds, although these have different ground states and band structures. The horizontal stripe structure with some inhomogeneity was observed in α-(BEDT-TTF)$_2$I$_3$ and α-(BEDT-TTF)$_2$KHg(SCN)$_4$, and the vertical stripe was observed in α-(BEDT-TTF)$_2$RbHg(SCN)$_4$. I found that the charge stripe structure is determined by the anisotropy of the Coulomb interaction, which is simply described by a parameter D_1/D_2, where D_1 and D_2 are distances between nearest neighbors for the α-type donor arrangement regarded as an anisotropic triangular lattice. I found that the boundary between the horizontal and vertical charge stripes are located between the D_1/D_2s for α-(BEDT-TTF)$_2$KHg(SCN)$_4$ and α-(BEDT-TTF)$_2$RbHg(SCN)$_4$.

The charge stripe is expected to be affected by hydrogen bonds between hydrogens of BEDT-TTFs and anions in the anion layer. It can be explained as the effect of hydrogen bonds, that the horizontal stripe for α-(BEDT-TTF)$_2$KHg(SCN)$_4$ is accompanied by some inhomogeneity, and the vertical stripe for α-(BEDT-TTF)$_2$RbHg(SCN)$_4$ develops well, since the vertical stripe is stable under the potential originates from hydrogen bonds when the off-site Coulomb interaction is negligible.

Moreover, it was observed the dimerization in the direction perpendicular to the charge

alignment of the charge stripe in α-(BEDT-TTF)$_2$I$_3$ and α-(BEDT-TTF)$_2$RbHg(SCN)$_4$ where the charge stripe has less inhomogeneity. The charge stripe is found to be stabilized by forming the dimerization.

Acknowledgments

There are many people who I would like to thank for their support during my life at Hokkaido University. I would like to express my deep gratitude to my supervisor, Associate Prof. K. Ichimura. His wide knowledge and his logical way of thinking have been great value for me. I would like to thank to Prof. S. Tanda of Hokkaido University for helpful advice and interesting idea of topological science. I would like to thank to Associate Prof. N. Matsunaga and Prof. K. Nomura of Hokkaido University for helpful advices, useful discussions and teaching me many phenomena of strongly correlated systems. I would like to acknowledge to Prof. M. Oda and Assistant Prof. T. Kurosawa of Hokkaido University for STM measurement, fruitful discussion and the method of analysis of STM images. I would like to thank to Prof. A. Kawamoto for useful advices for sample synthesis.

I would like to thank to Prof. K. Yamaya and Prof. S. Takayanagi of Hokkaido University for helpful instructions of low temperature resistivity measurement and prepareing stals. I would like to thank to Assistant Prof. T. Matuura of Hokkaido University for helpful instructions of low temperature resistivity measurement. I would like to acknowledge to Associate Prof. K. Yamamoto of Okayama University of Science for providing high quality samples of α-(BEDT-TTF)$_2$I$_3$. I would like to thank for members of laboratory of topological science and technology to daily supports and encouragements.

References

[1] E. Wigner, Phys. Rev. **46**, 1002 (1934).

[2] C. C. Grimes, and G. Adams, Phys. Rev. Lett. **42**, 795 (1979).

[3] C. C. Grimes, Surf. Sci. **98**, 1 (1980).

[4] K. Kanoda, Hyperfine interact. **104**, 235 (1997).

[5] K. Miyagawa, A. Kawamoto, and K. Kanoda, Phys. Rev. B **62**, R7679 (2000).

[6] T. Ishiguro, K. Yamaji and G. Saito. *OrganicSuperconductors*, Springer (Berlin 1998).

[7] D. Jerome, A. Mazaud, M. Ribault and K. Bechgaard, J. Physique Lett. **41**, L95 (1980).

[8] H. Urayama, H. Yamochi, G. Saito, K. Nozawa, T. Sugano, M. Kinoshita, S. Sato, K. Oshima, A. Kawamoto and J. Tanaka, Chem. Lett. **17**, 55 (1988).

[9] H. Seo, J. Phys. Soc. Jpn. **69**, 805 (2000).

[10] R. Kato, H. Kobayashi, A. Kobayashi, and Y. Nishio, Chem. Lett. 957-960 (1986).

[11] H. Mori, S. Tanaka, and T. Mori, Phys. Rev. B **57**, 12023 (1998).

[12] Y. Ihara, H. Seki, A. Kawamoto, J. Phys. Soc. Jpn. **82**, 083701 (2013).

[13] J. Merino, and R. H. Mckenzie, Phys Rev. Lett. **87**, 2370002 (2001).

[14] K. Hiraki, and K. Kanoda, Phys. Rev. Lett. **80**, 4737 (1998).

[15] D. Jerome, Science **252**, 1509 (1991).

[16] B. Salameh, S. Yasin, M. Dumm, G. Untereiner, L. Montgomery, and M. Dressel, Phys. Rev. B **83**, 205126 (2011).

[17] T. Kawai, and A. Kawamoto, J. Phys. Soc. Jpn. **78**, 074711 (2009).

[18] T. Kakiuchi, Y. Wakabayashi, H. Sawa, T. Takahashi, T. Nakamura, J. Phys. Soc. Jpn. **76**, 113702 (2007).

[19] Y. Yue, K. Yamamoto, M. Uruichi, C. Nakano, K. Yakushi, S. Yamada, T. Hiejima, and A. Kawamoto, Phys. Rev. B **82**, 075134 (2010).

[20] M. Watanabe, Y. Node, Y. Nogami, and H. Mori. Synth. Met. **135**, 665.

[21] Y. Nogami, and S. Kagoshima, Synth. Met. **16**, 376-377 (1986).

[22] F. Nad, P. Monceau, and H. M. Yamamoto, Phys. Rev. B **76**, 205101 (2007).

[23] S. Iwai, K. Yamamoto, A. Kashiwazaki, F. Hiramatsu, H. Nakayama, Y. Kawakami, K, Yakushi, H. Okamoto, H. Mori, and Y. Nishio, Phys. Rev. Lett. **98**, 097402 (2007).

[24] M. Watanabe, Y. Noda, Y. Nogami and H. Mori, Synth. Met. **135**, 665 (2003).

[25] H. M. Van Horn, Phys. Rev. **157**, 342 (1967).

[26] E. Y. Andrei, G. Deville, D. C. Glattli, and F. I. B. Williams, Phys. Rev. Lett. **60**, 2765 (1988).

[27] V. J. Goldman, M. Santos, M. Shayegan, and J. E. Cunningham, Phys. Rev. Lett. **65**, 2189 (1990).

[28] F. I. B. Williams, P. A. Wright, R. G. Clark, E. Y. Andrei, G. Deville, D. C. Glattli, O. Probst, B. Etienne, C. Dorin, C. T. Foxon, and J. J. Harris, Phys. Rev. Lett. **66**, 3285 (1991).

[29] M. A. Paalanen, R. L. Willett, R. R. Ruel, P. B. Littlewood, K. W. West, and L. N. Pfeiffer, Phys. Rev. B **45**, 13784 (1992).

[30] Y. Takano, K. Hiraki, H. M. Yamamoto, T. Nakamura, and T. Takahashi, J. Phys. Chem. Solids **62**, 393-395 (2001).

[31] P. Guionneau, C. J. Kepert, G. Bravic, D. Chasseau, M. R. Truter, M. Kurmoo, and P. Day, Synth Met. **86**, 1973 (1997).

[32] Z. Z. Wang, J. C. Girard, C. Pasquier, D. Jerome, and K. Bechgaard, Phys. Rev. B **67**, 121401(R) (2003).

[33] Y. Nogami, R. Moret, J.-P. Pouget, Y. Yamamoto, K. Oshima, K. Hiraki, and K. Kanoda, Synth. Met. **102**, 1778 (1999).

[34] K. Kajita, Y. Ojiro, H. Fujii, Y. Nishino, H. Kobayashi, A. Kobayashi, and R. Kato, J. Phys. Soc. Jpn. **61** 23 (1992).

[35] N. Tajima, S. Sugawara, M. Tamura, Y. Nishio, and K. Kajita, J. Phys. Soc. Jpn. **75**, 051010 (2006).

[36] S. Endo, Y. Watanabe, T. Sasaki, T. Fukase, and N. Toyoda, Synth. Met. **86**, 2013-2014 (1997).

[37] H. Mori, S. Tanaka, M. Oshima, G. Saito, and T. Mori, Bull. Chem. Soc. Jpn. **63**, 2183-2190 (1990),

[38] P. F. Henning, J. S. Brooks, J. E. Crow, Y. Tanaka, T. Kinoshita, N. Kinoshita, M. Tokumoto, and H. Anzai, Solid State Commun. **95**, 691-694 (1995).

[39] G. Binnig, H. Rohrer, Ch. Gerber and E. Weibel, Phys. Rev. Lett. **49**, 57 (1982).

[40] K. Ichimura, S. Ikeda, M. Kawai, K. Nomura, J. Ishioka, and S. Tanda, Physica B **404**, 570-572 (2009).

[41] S. Moroto, K. -I. Hiraki, Y. Takano, Y. Kubo, T. Takahashi, H. M. Yamamot, and T. Nakamura, J. Phys. IV France **114**, 339 (2004).

[42] E. Mori, H. Usui, H. Sakamoto, K. Mizoguchi, and T. Naito, J. Phys. Soc. Jpn. **81**, 014707 (2012).

[43] M. Ishida, K. Hata, T. Mori, and H. Shigekawa, Phys. Rev B, **55**, 6773 (1997).

[44] K. Yamamoto, A. A. Kowalska, and K. Yakushi, Appl. Phys. Lett. **96**, 122901 (2010).

[45] P. F. Leylekian, J. P. Pouget, Y. J. Lee, R. M. Nieminen, P. Ordejon and E. Canadell, Phys. Rev. B **82**, 134116 (2010).

[46] K. Noda, Y. Ihara, and A. Kawamoto, Phys. Rev. B **87**, 085105 (2013).

[47] P. Alemany, J. P. Pouget, and E. Canadell, Phys. Rev. B, **85**, 195118 (2012).

[48] M. Watanabe, Y. Noda, Y. Nogami and H. Mori, Synth. Met. **135**, 665 (2003).